Construction and Building Materials 341 (2022) 127824

Contents lists available at ScienceDirect

Construction and Building Materials

journal homepage: www.elsevier.com/locate/conbuildmat

Behaviour of clamp-enhanced palm tendons reinforced concrete

Emmanuel Owoichoechi Momoh, Adelaja Israel Osofero *, Oleksandr Menshykov

School of Engineering, University of Aberdeen, Kings College, Aberdeen, United Kingdom

ARTICLE INFO

Keywords:
Concrete Damage Plasticity
OPBF
Reinforced concrete
Bond pull-out
Flexural strength
Low-cost housing
Finite element analysis
Palm fibres

ABSTRACT

Recent studies on affordability and sustainability of building materials have shown that broom fibres derived from the leaflets of oil palm tree have impressive tensile strength but poor bond strength with concrete. Although bonding has been reported to be improved when the fibres are combined in the form of tendons, the bond-slip failure between the tendons and concrete still compromises composite performance. This study, therefore, investigates the use of hose clamps in increasing slip resistance between oil palm broom fibres (OPBF) tendons and concrete matrix. A total of 64 concrete samples comprising of 46 beams (100x100x500 mm) reinforced with varying areas of OPBF tendons and 18 bond pull – out samples were prepared. The tendon reinforcements were fitted with hose clamps to improve the bond strength between the concrete and the reinforcement. Spacing between hose clamps was chosen as 45 mm and 85 mm. The flexural strength of the beams was tested under 4-point bending at 28, 56 and 112 days. Test results show improvement in the flexural capacity of the beams as a result of increased slip resistance induced by the hose clamps. Finite element modelling of the behaviour of the OPBF-tendon reinforced concrete was carried out and recommendations were made after ensuring that the ultimate and serviceability limit states are satisfied.

1. Introduction

The need for alternative construction materials that are both economically and environmentally sustainable cannot be over-emphasised. Factors such as rising construction cost, high cost of urban land, weak land tenure system and lack of affordable housing finance have made it almost impossible for low and average income earners in developing countries to afford decent housing [1]. In the year 2000, Africa's population was estimated at 294 million and is projected at 742 million by 2030 with over 70% of its present urban population residing in slum settlements [2]. In most developing countries like Nigeria for instance whose total housing deficits is currently in excess of 22 million units (i.e., an increase of 15% from 2019) [3], conventional construction materials like reinforced concrete are expensive due to the importation of building materials such as reinforcing steel that is unavailable locally. The prevalence of slum settlements breeds inequality, poverty, and creates enabling environments for disease outbreaks in these countries [4], hence the need for locally available, affordable and environmentally friendly materials. Developing alternative building materials would lower construction costs while eliminating over-dependence on imported ones some of which are energy-intensive and possess high carbon footprint due to manufacturing and transportation (e.g. steel).

Studies have identified several natural materials which could serve as low-cost options for the use of steel reinforcement. These include the use of vegetable fibres such as coconut coir and oil palm fibres for residential building applications [5 6 7], *Grewia otiva* and *Pinus roxburghii* fibres in reinforcing adobe [5], fan palm fibre for reinforcement of concrete [6], sisal and eucalyptus fibres for reinforcing cement-based roofing tiles [7], sisal fibre reinforced cement-based roofing components [8], etc. These fibres are used in discrete form, randomly dispersed in cementitious matrices and have been reported to improve the mechanical properties of the resulting composite. Although drawbacks exist such as the embrittlement of the fibres by the alkaline environment of cementitious matrices [9] and dimensional instability due to hydrophilicity of cellulose such that the bonding between fibre and matrix is compromised [10], studies have also shown how these drawbacks could be mitigated, for example, through thermal and chemical treatments [11 12].

Vegetable fibres are usually recommended to be used as randomly distributed discrete fibre reinforcements, except bamboo and broom briskets (from oil palm tree) which have shown some prospects for use as longitudinal reinforcement in concrete [61]. In fact, bamboo is asserted to be superior to steel in terms of strength-to-weight ratio [12 16 17] and has enjoyed numerous research attention for its application in beams, columns and slabs. Ghavami [13] in the study of the flexural behaviour

* Corresponding author at: School of Engineering, University of Aberdeen, UK.
E-mail addresses: r01eom18@abdn.ac.uk (E.O. Momoh), aiosofero@abdn.ac.uk (A.I. Osofero), o.menshykov@abdn.ac.uk (O. Menshykov).

https://doi.org/10.1016/j.conbuildmat.2022.127824
Received 19 August 2021; Received in revised form 28 April 2022; Accepted 8 May 2022
Available online 19 May 2022

Nomenclature

f_c	is the uniaxial compressive strength of concrete
f_t	is the uniaxial tensile strength of concrete
f_{cu}	is the maximum uniaxial compressive strength of concrete
f_{cm}	is the mean concrete strength in uniaxial compression
f_{tu}	is the maximum uniaxial tensile strength of concrete
ε_{cu}	is the maximum strain of concrete in uniaxial compression
$\varepsilon_o^{'}$	is strain of concrete at maximum uniaxial compressive stress f_{cu}
ε_o^{el}	is elastic strain of concrete in uniaxial compression
ε_{of}^{el}	is the elastic strain of OPBF tendon in tension
ε_f^{in}	is the inelastic strain of OPBF tendon in tension
ε^{in}	is the inelastic strain of concrete
E_o	is the undamaged elastic stiffness of concrete
E	is the post-elastic stiffness of concrete
E_{of}	is the undamaged elastic stiffness of OPBF tendon
E_{fc}	is the damaged stiffness of OPBF tendon in compression
d_c	is the compression damage parameter of concrete
d_t	is the tension damage parameter of concrete
ε_t	is the tensile strain of concrete
ε_{cr}	is the cracking strain
ε^{pl}	is the plastic strain
n	is the calibration parameter for stress–strain response of concrete in tension
ϵ	is the eccentricity
ψ	is the dilation angle of material
f_{bo}	is the concrete strength in biaxial compression
f_r	is the modulus of rupture of concrete
f_f	is the uniaxial tensile strength of OPBF tendon
f_{fT}	is the maximum uniaxial tensile strength of OPBF tendon
f_{fTd}	is the design tensile strength of OPBF tendon
f_{fc}	is the maximum compressive strength of OPBF tendon
f_{yd}	is the design strength of the steel reinforcement
A	is the area of steel reinforcement
A_f	is the area of OPBF tendon reinforcement
ε_T	is the tensile strain at f_{fT}
ε_T^{in}	is the inelastic strain of OPBF in uniaxial tension
ε_c^{in}	is the inelastic strain of OPBF in uniaxial compression
ε_{cT}	is the total compressive strain of OPBF tendon
ε_{of}^{el}	is the elastic strain of OPBF in uniaxial tension
ε_{oc}^{el}	is the elastic strain of OPBF in uniaxial compression
E_{oc}	is the undamaged elastic compressive stiffness of OPBF tendon
E_f	is the post-elastic stiffness of the OPBF tendon in tension
d_{Tf}	is the tension damage parameter of OPBF tendon
d_{cT}	is the compression damage parameter of OPBF tendon
ε_T^{pl}	is the plastic strain of OPBF tendon
k_{nn}	is the cohesive stiffness in the normal direction
k_{ss}	is the cohesive stiffness in the shear direction
k_{tt}	is the cohesive stiffness in the tangential direction
A_f	is the area of OPBF tendon reinforcement
z	is the lever arm of reinforcing material
F	is the number of OPBF in a tendon
d_x	is the effective depth of reinforcement
M	is the moment capacity of section
z	is the lever arm of the section
P_{max}	is the maximum pull-out force
L_b	is the embedded length of tendon
d_b	is the cross-sectional diameter of tendon
$\alpha, \beta, \gamma, \lambda_1$ and λ_2	are real constants of OPBF stress–strain constitutive behaviour

of bamboo (*Dendrocalamus giganteus*) reinforced lightweight concrete (with characteristic compressive strength of 19 MPa) reported up to 400% improvement in ultimate flexural strength of 120x300x3400mm beams. The surfaces of the bamboo strips were waterproofed with Negrolin (a water-based asphalt paint). The study recommended a maximum reinforcement ratio of 3%. Agarwal et al. [12] studied the feasibility of reinforcing M20 concrete with treated bamboo (*Melocanna bambusoides*) strips through a bond pull-out test, compressive and flexural tests. The bamboo strips were pre-treated by coating their surfaces with adhesives such as Tapecrete P-151, Araldite, Sikadur 32 Gel and Corr RC. Sikadur 32 Gel proved to be the best coating for the reinforcing strips resulting in over 300% improvement in bond strength. Improvement in flexural capacities of the 75x150x1000mm beams was up to 29% with a bamboo reinforcement ratio of 1.49%. The study also reported that 8% bamboo reinforcement ratio was equivalent to a 0.89% of steel reinforcement ratio in terms of axial and lateral resistance for a 150 × 150 × 1000 mm concrete column.

Qaiser et al. [14] studied the flexural behaviour of 230x230x1880mm bamboo reinforced concrete beams. The bamboo strips were treated by applying a helical winding of steel wire and by corrugating the surface of the strips using mechanical means. The beams reinforced with the corrugated bamboo strips showed up to 80% improvement over the plain bamboo reinforced beams. Maximum bond strength of 0.29 MPa was recorded between the bamboo and concrete strips and a reinforcement ratio of 4% was adopted for the 17 MPa concrete based on the similarities in cracks pattern.

Mali and Datta [15] carried out an experimental evaluation of concrete slabs reinforced with bamboo (*Bambusa arundinacea*) strips. The slabs had a plan dimension of 600x600mm and a thickness of 100 mm. Three categories of 20x10mm bamboo strips were used as reinforcement: i.e., plain untreated strips, plain treated strips, and grooved treated strips. The strips were firstly dipped in chemical adhesive and thereafter wrapped with 1 mm steel wire over the strips in a helical form. The concrete used had a characteristic strength of 28 MPa while the spacing of the strips was 100 mm centre to centre in both directions. In terms of flexural strength, the bamboo reinforced concrete performed 1.5–2 times better than the unreinforced concrete. The grooved treated bamboo had the best performance with energy absorption being over 45% of the steel-reinforced slabs. The bamboo reinforced concrete slabs also showed similar failure pattern as the steel reinforced slabs. Although the grooved bamboo strips were recommended for use as structural reinforcement under limited gravity loading situation, durability concerns exist due to possible loss of concrete-bamboo bond with time.

The overall performance of cementitious composites like concrete is dependent on the bond between matrix, reinforcement, and other complex interactions governing the value of fracture energy, occurrence of localised deformations, level of chemical adhesion, and the magnitude of frictional force and mechanical interlock [16]. The highest contribution to bonding between concrete and reinforcement arises from mechanical interlock [17]. Due to the surface conditions of steel reinforcement, sufficient bond is maintained with concrete thereby maintaining strain compatibility at the reinforcement depth. However, for most reinforcements of vegetable origin like bamboo-reinforced concrete, composite performance is usually compromised by the loss of bond between the reinforcement and concrete. This results in excessive service deflections and reduced load capacities. This is further made worse with time-induced embrittlement of the reinforcement due to the

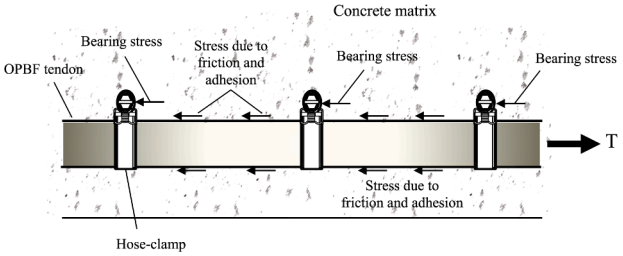

Fig. 1.1. Simplified conceptualisation of bond stress distribution for a hose-clamp fitted reinforcement tendon in concrete.

presence of alkali in the cement thereby invalidating the usual design equations. Among methods reported for enhancing the bond between concrete and bamboo reinforcements, are notching of the bamboo reinforcement strips [14], use of epoxy coating on the reinforcement surface [18], a combination of grooving of reinforcement surface by mechanical means, coating with chemical adhesive and sand-blasting [15] helical wire winding around the reinforcement strips, water-proofing [13 14], use of studs [19] and use of hose clamps [20].

While bamboo has enjoyed the expected research attention as a natural material for the longitudinal reinforcement of concrete, only very little is known about OPBF. Recent studies have shown that broom briskets derived from the oil palm tree (*Elaeis guineensis*) possess mechanical properties similar to bamboo and is also superior to steel in terms of tensile strength/weight ratio [21 22]. Preliminary characterisation of OPBF can be found in a previous study of Momoh et al. [23]. Although this tensile strength capacity can only be attained along the grains, the study opined that more than one OPBF can be twisted around one another in the longitudinal direction in a helical form to produce tendons. This procedure resulted in a boost in radial rigidity of the tendons. The use of OPBF in a combined tendon form was also suggested in a subsequent study which investigated the bond pull-out behaviour of single OPBF and OPBF tendons in C30 concrete at 28, 56 and 112 days [24]. The tendons were prepared by winding single OPBF around one another in the form of a helix after which the tendons were embedded in concrete to a length of 80 mm. In this form, bond strength of up to 1.16 MPa representing 46% improvement (in comparison with the single OPBF) was reported.

The problem with this method however is the difficulty in reproducing the tendons on-site by merely winding the individual fibres over one another. Secondly, the mere winding of the fibres did not achieve much rigidity of the tendons due to low radial stiffness. Furthermore, a reduction of bond strength with time was reported due to the cement alkali-induced degradation of the OPBF surface at the fibre-concrete interface. The studies of Momoh et al. [11 25] reported attempts to mitigate fibre surface degradation by 3 pre-treatment methods, namely: soaking the OPBF tendons in (i) sodium hydroxide, (ii) triethoxyvinylsilane, and (iii) boiling water. The studies recommended optimum treatments of either soaking the OPBF in 6% NaOH for 48 h, or in 3% triethoxyvinylsilane for 24 h, or by boiling the OPBF in water at 100 °C for 30 min. Improvement in bond strength of 37% was reported for the silane-treated tendons with concrete at 112 days, which implies that the durability of the OPBF tendons can be improved through the prescribed pre-treatments. However, the reported maximum bond strength of only 1.12 MPa may not be sustained in the long-term as the OPBF tendons will still have to resist alkali-induced degradation beyond 112 days.

Consequently, a more practical method of adequately mobilising the strength of the individual fibres into tendon units has become imperative. The use of hose clamps has therefore been employed in this study to tie individual fibres together to form tendons. The attachment of hose clamps unto OPBF tendons would also provide shear connection between the OPBF tendons and concrete matrix. The consequent composite action between the clamps, tendon and concrete would be

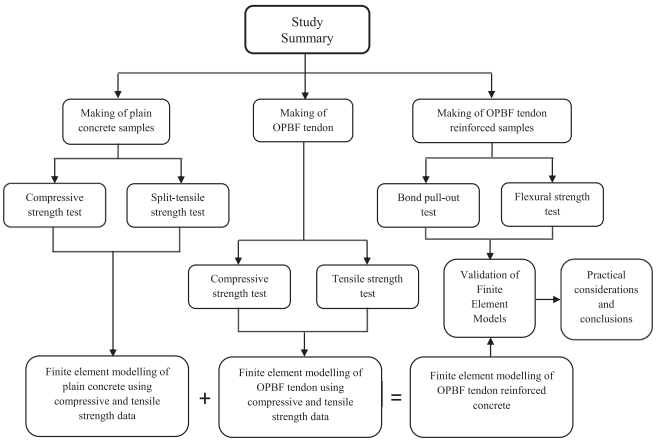

Fig. 2.1. Summary of tasks carried out in the study.

advantageous for mechanical interlocking, slip resistance, bond strength, energy dissipation and the flexural capacity of the OPBF-reinforced concrete elements. Fig. 1.1 presents a simplified concept of bond stress distribution for a tendon (fitted with hose clamps) in a concrete matrix [61]. The use of hose-clamps to maximise bond strength between OPBF and concrete would lead a new line of research in alternative reinforcements, and hence ease pressure not only on steel but on already popularly researched alternatives like bamboo. The concept of providing shear connection on longitudinal reinforcement if extended to fibre reinforced polymer (FRP) bars reinforced concrete could solve the poor bond problem of FRP bars and could reveal an interesting composite behaviour. This study therefore seeks to investigate the behaviour of concrete reinforced with OPBF tendons that have been enhanced with steel hose clamps as well as employ finite element modelling in predicting the bond and flexural behaviour of the composite.

This study commenced with an experimental programme in Section 2, where individual OPBF were combined in the longitudinal direction, then fitted with hose clamps to form OPBF tendons (as depicted in Fig. 1.1). Tensile strength test was then performed on the tendons to study their tensile behaviour and to determine their ultimate tensile strengths. Similarly, compressive strength test was also performed on tendon units (i.e., short tendons consisting of hose clamps at both ends). Fresh concrete was prepared from which concrete cubes and cylinders were cast to determine the plain concrete compressive and tensile strengths respectively. Bond pull-out behaviour of the OPBF tendons was then studied to determine the bond strength of the OPBF tendons from concrete. After the assessment of bond behaviour, concrete prisms were cast embedded with OPBF tendon reinforcements, after which the flexural behaviour of the OPBF tendon reinforced beams was studied. Discussion of the results of the various experiments are presented in Section 3. Finally, finite element modelling of the behaviour of the OPBF tendon reinforced concrete was carried out using the concept of concrete damage plasticity (CDP) and compared to the results from the experiments. The study is concluded in Section 4 with recommendations made such that ultimate and serviceability limit states are satisfied.

2. Experimental programme

The summary of the experiments/tasks carried out in this study is shown in the flowchart of Fig. 2.1 below:

2.1. Materials and methods

Oil palm broom fibres were purchased from *Rice and Spice*, Aberdeen, UK in form of broom units. The approximate age of the fibres is about 400 days after harvesting. The fibres were air-dried to the moisture

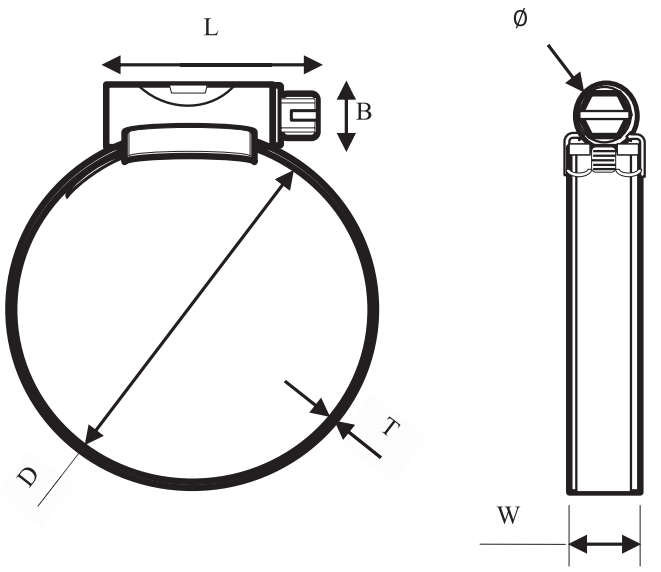

Fig. 2.2. Side views of steel hose clamps.

content between 7 and 11%. At<7% moisture content, the fibres become brittle thereby making them difficult to handle. At a moisture content of 9%, the density of OPBF was obtained as 840 kg/m^3. All OPBF used in this study were not subjected to any form of treatment. Hose clamps made of mild steel were obtained from *RS-component Ltd*, Aberdeen, UK. Fig. 2.2 and Table 2.1 illustrate the dimensions and torque requirements of the clamps used for each of the reinforcement tendons.

The binder and aggregates were obtained from *Jewson Ltd*, Aberdeen, UK. General-purpose cement (Blue Circle) was used as the binder while sand and gravel were used as the fine and coarse aggregates respectively. The specific gravities of the aggregates were determined according to the requirements of ASTM D854-14 [26]. Specific gravities of cement, fine aggregate and coarse aggregates were determined as 3.15, 2.55 and 2.62 respectively. The analysis of particle sizes of the fine and coarse aggregates carried out according to the requirements of ASTM D2487 [27].

The sand was classified as *medium sand* and the gravel as *fine gravel* having a maximum particle size of 10 mm.

Concrete grade of C30 which is representative of concrete used for the construction of residential buildings was used for making the samples. A mix proportion of 1:1.5:3 of cement, sand and gravel respectively was used for the preparation of the concrete with water-cement ratio kept constant as 0.52. Mixing of cement and aggregate for concrete was carried out in an electrically powered concrete mixer with a capacity of 30 L. Details of aggregate grading and mix used for this study is the same as used in earlier works by the authors [22]. The concrete was prepared and tested in compression according to ASTM C192/C192M-02 [28], in tension according to ASTM C496/C496M-17 [29], and in flexure according to ASTM C1609/C1609M-12 [30]. Average compressive strength of the 3 (100x100 x100mm) plain concrete was 40 ± 2 MPa. Average tensile strength of the 3 (100⌀x200mm) plain concrete cylinders was 3.45 ± 0.1 MPa and the average flexural strength of the 3 (100x100x500mm) plain concrete prisms was 4.04 ± 0.2 MPa.

2.2. Tensile strength test of OPBF tendons

OPBF without blemish were selected by physical inspection and cut into lengths of 250 mm. In order to enhance the rigidity of the fibres, the fibres were held side-by-side in the longitudinal direction in the form of tendons using hose clamps. Two hose clamps were used to hold the tendons at a spacing of 90 mm (gauge length). A torque wrench was used to tighten the hose clamps on to the tendons to a torque of 3.5 ± 0.2 N-m. Stainless steel wire rope was untwined to extract the individual steel wires which were then inserted across the cross-section of the smeared ends of the tendons. After this, a steel o-clip was inserted on the same end. The steel wire now situated at the bottom of the o-clips was raised and passed over the o-clips and through the tendon cross-section. This procedure was repeated for all four o-clips at both ends of the tendon samples and has been illustrated in Fig. 2.3. Both ends of the tendons beyond the gauge length were soaked in Araldite epoxy glue after which the clipped ends were flattened to about 10 mm thickness using a plier to enable insertion into the machine grip. The tendons were left for 72 h so that the glue could set before carrying out the test. This procedure ensured that the tendons acted as one unit (at least at the grips) so that the tensile force from the grips of the machine was adequately applied across the tendon cross-section.

After adequate curing of the adhesive applied on to the samples, steel pipe clamps were tied firmly on to the 2 hose clamps used to hold the tendons (refer to Fig. 2.3). A steel bosshead was then screwed on to the threaded stud of each pipe clamp such that the bottom bosshead held the linear variable displacement transducer (LVDT) device while the top bosshead held a horizontal flat aluminium surface from which the tip of the LVDT device measured the extension of the tendons under axial tensile loading. Testing was carried out at 5 mm/min until failure of the tendons. Three identical samples were tested.

For the reinforcement tendons, the fibres were first cut to a length of 480 mm. In terms of the number of fibres, three categories of fibres were investigated: 40 fibres-tendon, 80 fibres-tendon and 120 fibres-tendon. In terms of spacing of hose clamps, two spacings were adopted: 45 mm and 85 mm such that 040F-45 s refers to a tendon consisting of 40 fibres and whose clamps are spaced at 45 mm. Similarly, 120F-85 s refers to a tendon consisting of 120 fibres and whose clamps are spaced at 85 mm. A torque wrench was used to tighten the hose clamps on to the tendons to a torque of 3.5 ± 0.2 N-m.

2.3. Compressive strength test of OPBF tendons

Due to the way several strands of fibres were combined into tendons, the compressive behaviour would be markedly different from the behaviour in tension. Hence compressive tests were also carried out. For the compressive strength test, OPBF without blemish were also selected by physical inspection and cut into lengths of 500 mm for easy handling. Hose clamps were used to hold the fibres side-by-side in the longitudinal direction to form tendons. Two (2) categories of tendons were tested in compression: these are the tendons with 45 mm spacing and the tendons with 85 mm spacing. The 85 and 45 mm spacing of hose clamps were adopted to evenly accommodate 6 and 10 hose clamps respectively within the 500 mm prism length for the flexural test samples. A torque wrench was used to tighten the hose clamps on to the tendons to a torque of 3.5 ± 0.2 N-m. The 2 categories of tendons were then cut into units with each unit comprising hose clamps at both ends, therefore making

Table 2.1
Dimensions and specifications of hose clamps used in the study.

Tendon* category	Internal diameter (D) mm	Width (W) mm	B mm	L mm	⌀ mm	Thickness (T) mm	Screw bolt	Torque range N-m
40F	9.5 – 12	9.0	10.0	11.0	6.0	0.6	Slotted Hexagonal	3 – 4
80F and 120F	11 – 16	9.0	10.0	21.0	7.0	0.7	Slotted Hexagonal	3.5 – 5

*40F means 40 OPBF/tendon.

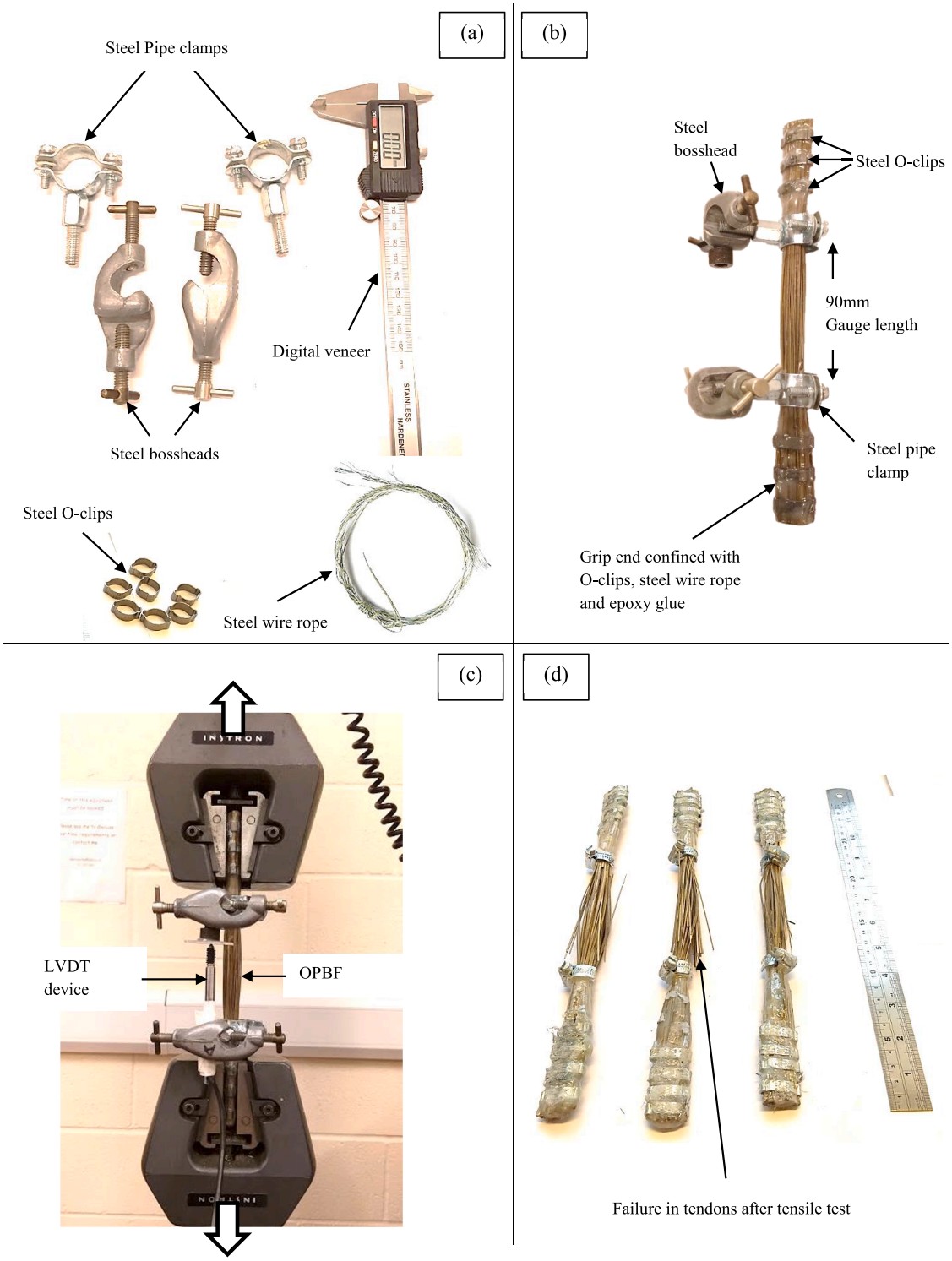

Fig. 2.3. Illustration of (a) items used for sample preparation for tensile test of OPBF tendons, (b) tendon set up, (c) tensile test set up, and (d) tendons after tensile testing.

the clamp spacing the gauge length of the specimens. The units were then tested for compression by applying an axial compressive load at a displacement control of 1 mm/min. Fig. 2.4a illustrates the units prepared for compression testing and Fig. 2.4b shows some damaged samples after the compressive test.

2.4. Bond pull-out test

The samples for bond strength consist of 100 mm cubic concrete and an OPBF tendon embedded to a length of 80 mm. The hose clamp enhanced tendons described in section 2.2 were cut into lengths of 250 mm. The bottom surface of the tendons was levelled using a hacksaw and then smeared with Araldite epoxy adhesive to enhance the rigidity of the surface for instrumentation. At the top of each tendon, a machine-

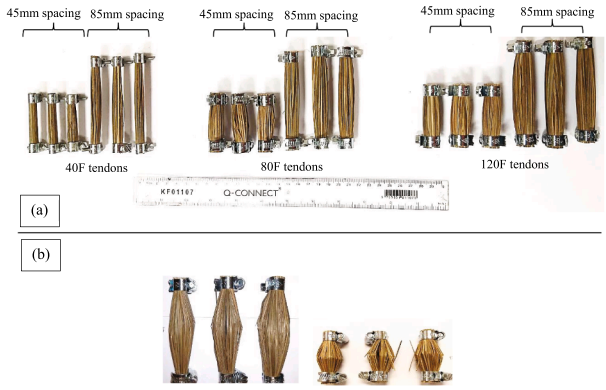

Fig. 2.4. OPBF tendon samples in basic units: (a) before compression test. (b) after compression test.

grip area was prepared by confining the tendons with 3 steel o-clips per end. This was achieved by spreading open the fibres at the top of the tendons, pouring in epoxy glue into the opening, then slotting in the o-clips and using a plier to flatten the o-clips unto the tendons such that a minor diameter of about 10 mm was obtained for the now oval (formerly circular) clips. This was done so that the end of the tendons could fit into the jaw of the machine. This procedure ensured that the tendons acted as one unit and the pull-out force from the grips of the machine was uniformly applied across the tendon cross-section. The result of not carrying out this procedure is that some or a portion of the fibres will be pulled out separately. The tendons were left for 72 h so that the adhesive could set before marking off the embedded length and inserting in concrete.

Fresh concrete was poured into the 100 mm cubic moulds, and a tendon was inserted in each mould containing concrete. Each tendon was held in the vertical position by hand while the concrete was vibrated for about 20 s on the vibrating table. Generally, vibration is deemed sufficient as soon as the surface of the concrete becomes relatively smooth and large air bubbles cease to break through the top surface [28]. The concrete surfaces were levelled using a hand trowel and the samples were left standing for about 24 h for adequate setting of the concrete. The samples were transferred into a curing tank with the water depth maintained at about 100 mm. This was done to avoid soaking of the tendons above the concrete. A total of 18 samples were cast for the bond pull-out investigation. The following nomenclature was used for sample identification, XF-Yc-Zd where X is the number of fibres per tendon, Y is the number of clamps and Z is the age of curing (in days) of the sample. For instance, 080F-2c-56d refers to a bond pull-out sample of 80 fibres/tendon, 2 embedded clamps and tested at 56 days. Similarly, 120F-1c-28d refers to a bond pull-out sample consisting of 120 fibres per tendon, 1 embedded clamp and tested at 28 days. Two identical samples each were prepared and tested for the bond pull-out tests. Although a single bond-pull out curve for each sample is presented in Fig. 3.3, the variation in bond strength can be seen in the standard deviations (represented by error bars) in Fig. 3.4.

The bond strength between the fibres and concrete matrix was measured at 28, 56 and 112 days through direct pull-out of the OPBF tendons from the concrete. At the respective maturity dates, the samples were taken out of the water, left standing for about 3 h to dry and then the underside opened to expose the end of the tendons. An LVDT device was inserted through this opening, touching the tendon. The test set up and illustrations are shown in Fig. 2.5.

The tendons were pulled out of the concrete matrix at the rate of 2.5 mm/min. Bond stress (u_f) can be calculated using Eq. (2.1):

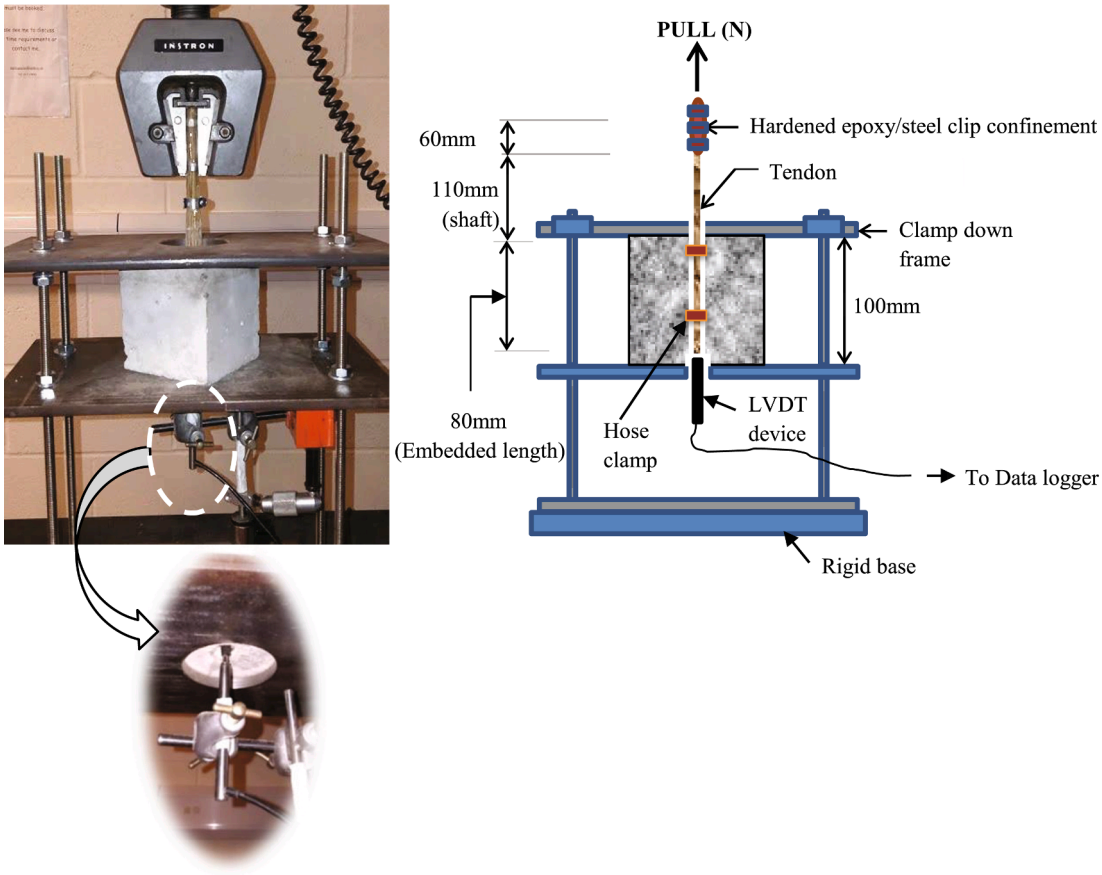

Fig. 2.5. Set up for pull-out test.

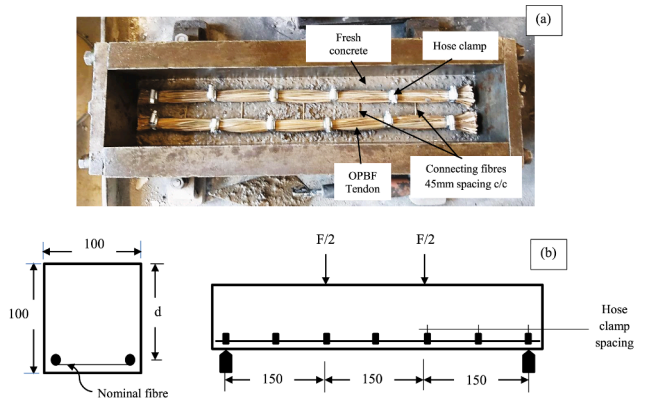

Fig. 2.6. (a): Illustration of OPBF tendon reinforcement in mould (b) Cross-section and longitudinal sections of an OPBF reinforced concrete sample.

$$u_f = \frac{P_{max}}{\pi d_b L_b}, \tag{2.1}$$

where, P_{max} is maximum pull-out load, d_b, the diameter of tendon cross-section and L_b is the embedded tendon length. This pull-out procedure is consistent with studies [31 32].

2.5. Flexural test of OPBF reinforced concrete

A singly reinforced section was attempted where the area of the reinforcement was varied by increasing the number of OPBF, i.e. in the three categories of 40F, 80F and 120F tendons. In terms of spacing of hose clamps, two spacings were adopted: 45 mm and 85 mm. Each reinforcement consisted of 2 tendons and 5 single fibres used for connecting the tendons. The spacing of the connecting fibres was set to 45 mm for all reinforcements (see Fig. 2.6a and 2.6b). Three tendon sizes and two clamp spacings were employed to observe possible effects of the reinforcement areas, spacings of the hose clamps and age (of curing of concrete) on the flexural response of the reinforced concrete beams.

The metallic moulds were placed on a vibrating table after which fresh concrete was poured into them to a depth of 10 mm and vibrated for about 20 s. The reinforcement was then placed in the moulds already containing the concrete such that the concrete cover to reinforcement was 10 mm. The rest of the concrete was then poured into the moulds to the full and vibrated for a further 60 s. After this, the sample surfaces were levelled with the aid of a hand trowel. The samples were then left to set for 24 h after which they were demoulded and transferred to the curing area. The samples were then covered with jute bags with tap water poured over the covering until it was wet. After this, a covering of polyethene material was laid over the jute covering to minimise evaporation of water. The wetting procedure was carried out every 2 days. Curing of the samples was done in the laboratory at room temperature for 28, 56 and 112 days. The following nomenclature was used for sample identification: XF-Ys-Zd. For instance, 040F-45 s-028d refers to a beam sample reinforced with 40 fibres, whose clamps are spaced at 45 mm and should be tested at 28 days.

At the respective maturity dates, the samples were removed from the curing area and left standing on a preparation table for about an hour to dry. The samples were then wiped clean using a toilet paper after which a marker was used to mark the points for the machine fixtures. An aluminium bracket was attached to the side of the samples at midspan. A test frame was mounted accordingly on these markings before transferring the samples onto the test machine. An LVDT device was inserted on the provision made on the test frame and positioned onto the side bracket on the samples to measure midspan deflection. The samples were then subjected to 4-point flexure according to ASTM C1609/C1609M-12 [30]. Although there exists no design guidance yet for this kind of research where small strands of materials are put together to act monolithically as longitudinal reinforcement in concrete, the ASTM C1609 provides a practicable starting point. Fig. 2.7 illustrates the flexural strength test set up. A total of 46 beam samples of 100x100x500mm were cast with varying OPBF reinforcement areas. Single samples were made and tested in flexure for the OPBF tendon reinforced concrete, hence single results are provided.

Two samples each of unreinforced and a steel-reinforced prisms (with ribbed 6 mm steel rebar) were also prepared in order to compare the behaviour of the palm tendon reinforced concrete. The steel rebars with modulus of elasticity of 200GPa and yield strength of 400 MPa (at a strain of 0.002) were purchased from *Wickes stores*, Dundee, UK. There was no provision for shear reinforcement for all samples. In order words, there was no use of stirrups used in this study. Furthermore, due to the nascent stage of this research, the overall flexural behaviour (from onset of loading to complete destruction) of the samples were taken into consideration since design guidance and recommendation cannot be carried out without a robust understanding of post-peak flexural behaviour.

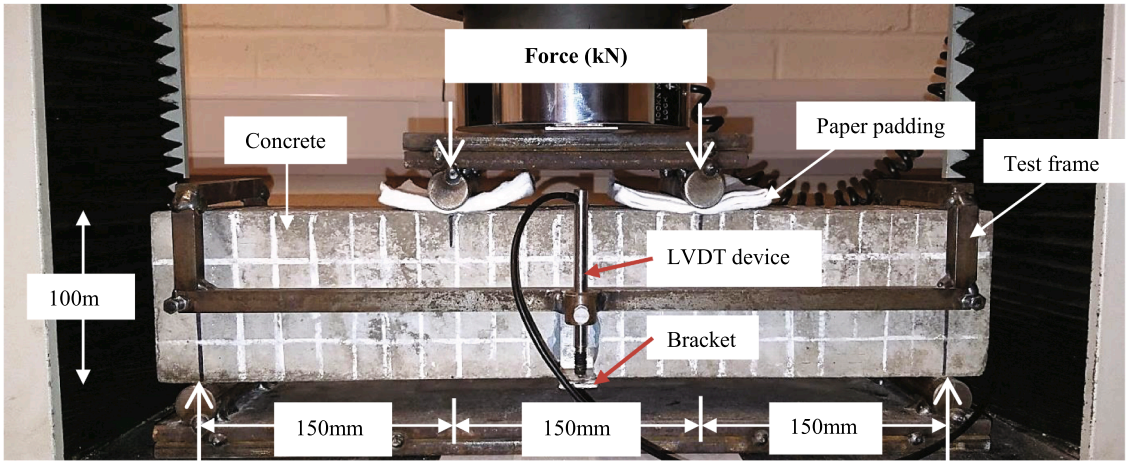

Fig. 2.7. The 4-point flexural strength set up.

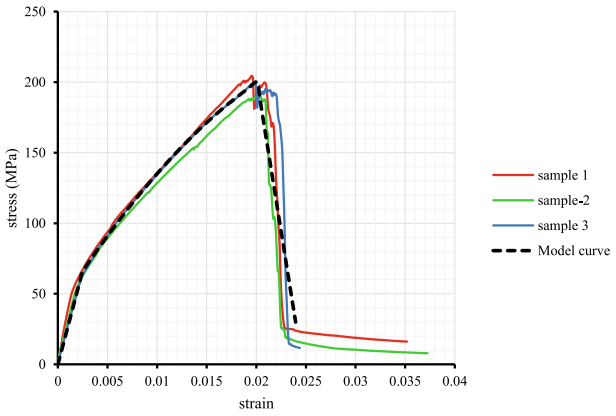

Fig. 3.1. Stress–strain curves of tensile tests of OPBF tendons.

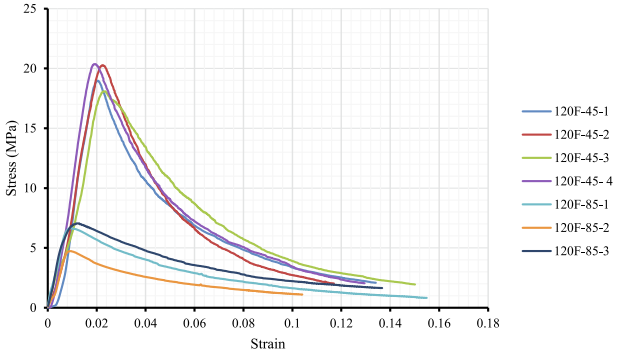

Fig. 3.2. Compressive strength of OPBF tendons.

3. Results and discussion

3.1. Behaviour of OPBF tendons

3.1.1. Tensile behaviour of OPBF tendons

Although the behaviour of single OPBF in uniaxial tension is approximately linear elastic, like most fibres of vegetative origin, the behaviour of the tendons can be better described as a "pseudo-inelastic" response. This is because the individual fibres in the tendon fail in a brittle manner at different stress levels. At the onset of loading, the tendons respond in a linear elastic manner. At some point, the slope of the stress–strain curve reduces as the first set of fibres fail thereby resulting in the transfer of stress on to a reduced section. This inelastic regime continues until most of the individual fibre fracture and a rapid deterioration of the stress–strain curve occurs. This is beneficial for the composite behaviour with concrete as sudden section failure of the concrete would be suppressed/eliminated. Average tensile strength of 198 MPa was recorded while Fig. 3.1 presents the stress–strain curves of the three tensile tests carried out and an idealised curve to model the uniaxial stress–strain relationship.

3.1.2. Compressive behaviour of OPBF tendons

Fig. 3.2 shows the compressive behaviour of the two categories of tendons. As loading commenced, fibre re-orientation within the tendons caused an initial low resistance to the compressive stress. As fibre re-orientation reaches an optimum, the resistance of the section is enhanced, and a stress hardening response is experienced where the slope of the stress–strain curve increases steadily. The modulus of elasticity of the section is then maintained until the peak compressive strength is reached. After the peak compressive stress, there is a rapid deterioration in strength as fibres buckle radially.

Fig. 2.4a and 2.4b show the different categories of tendons before and after compressive testing. Fig. 3.2 shows typical stress–strain curves for tendons whose clamps were spaced at 45 mm and 85 mm. The compressive strength of the fibres with 45 mm clamp spacing, was higher than that of the tendons with 85 mm clamp spacing. This is because a larger spacing implies a longer length of unconfined fibres thereby increasing fibre slenderness and hence reducing their critical buckling load.

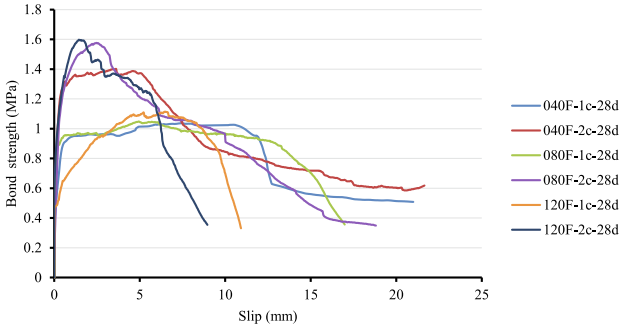

Fig. 3.3. Bond pull-out response of clamp enhanced OPBF tendons at 28 days.

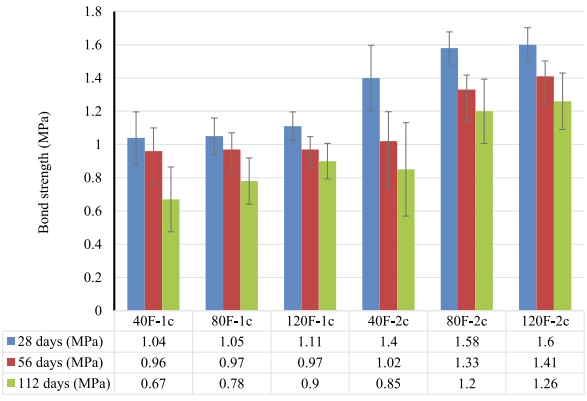

	40F-1c	80F-1c	120F-1c	40F-2c	80F-2c	120F-2c
28 days (MPa)	1.04	1.05	1.11	1.4	1.58	1.6
56 days (MPa)	0.96	0.97	0.97	1.02	1.33	1.41
112 days (MPa)	0.67	0.78	0.9	0.85	1.2	1.26

Fig. 3.4. Bond pull-out response of clamp enhanced OPBF tendons at 28, 56 and 112 days (error bars represent standard deviation of the bond strength values).

3.2. Bond pull-out behaviour of OPBF tendons

Bond pull-out behaviour of OPBF-tendons from concrete was characterised by an initial complete adhesion between the tendons and concrete. As the pull-out load increased, adhesion was lost, and the pull-out force was transferred onto the clamps. Beyond this stage, the grip of the clamps on the tendons was lost due to damage of circumferential fibres and the tendon slips through the concrete until complete pull-out. From the experiment, slip between the clamps and the concrete was observed to be negligible. Fig. 3.3 presents the experimental bond slip curve for all tendon categories at 28 days, while Fig. 3.4 shows a summary of the average maximum bond strengths (with error bars representing standard deviations) at 28, 56 and 112 days.

Maximum bond strength increased with the size of the tendons and the reduced clamp spacing. In the case of steel-reinforced concrete, however, bond strength reduces with increasing size of the rebars due to Poisson ratio effect [17 33], the case is different for OPBF tendons as an increase in bar diameter implies a corresponding increase in the number of fibres. Consequently, surface undulation increases, and more sites are created for friction and adhesion. Maximum bond strength of 1.6 MPa

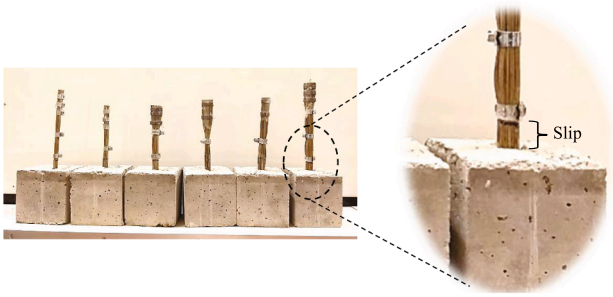

Fig. 3.5. Some bond pull-out samples after testing.

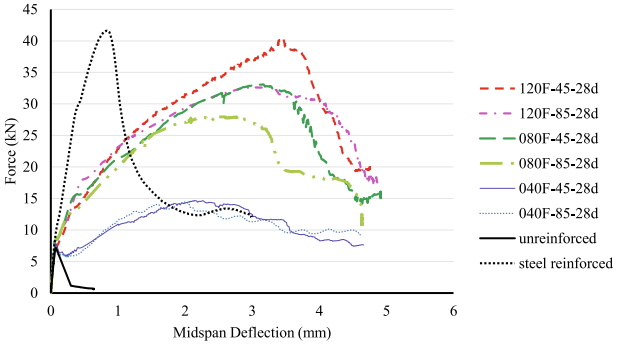

Fig. 3.6a. Flexural response of clamp enhanced OPBF reinforced concrete at 28 days.

was recorded for the 120F-2c-28d sample.

However, it was noticed that the bond strengths reduced with the age of the samples. The cement alkali-induced embrittlement of the OPBF surface is responsible for the drop in bond strength (Fig. 3.4). Images confirming the deterioration of OPBF in concrete after 112 days were obtained through scanning electron microscopy in an earlier study by Momoh et al. [24]. Generally, alkali-induced degradation is a major drawback to the use of natural fibres as reinforcement and corroborates the findings of previous studies [7 8 16]. While the proposed chemical and thermal methods of mitigating this drawback [6 11] have mainly been applied to discrete fibres, surface coating with structural grade adhesives and the use of mechanical attachments have yielded superior results on natural (longitudinal) reinforcements like bamboo strips [13 34 20].

A maximum reduction in bond strength of 27% and 39% was recorded at 56 days and 112 days respectively for the 40F-tendons, while the average reduction in bond strength across all tendon configurations was 14% and 27% at 56 days and 112 days respectively. This means that the loss of bond strength with time reduced with increase in the size of the tendons. The higher loss of bond with time for the 40F fibres is due to the fact that the percentage of total fibres forming the circumference of the tendons is greater than that for the 80F and 120F tendons. In order words, more of the fibres in 40F tendons were exposed to the concrete. As the circumferential fibres absorbed alkali from moisture in the surrounding concrete, the bond with the concrete was compromised due to degradation of tendon surface. Generally, a pull-out failure mode was experienced for all samples (see Fig. 3.5).

3.3. Flexural behaviour of OPBF reinforced concrete

The flexural behaviour of OPBF-reinforced concrete is characterised by an initial linear elastic response (pre-crack stage) after which cracking of concrete sets in and the slope of the force-midspan deflection

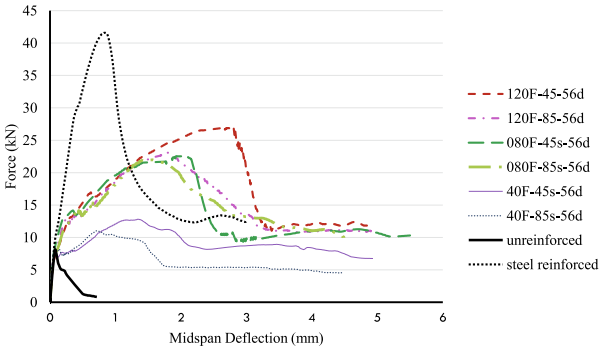

Fig. 3.6b. Flexural response of clamp enhanced OPBF reinforced concrete at 56 days.

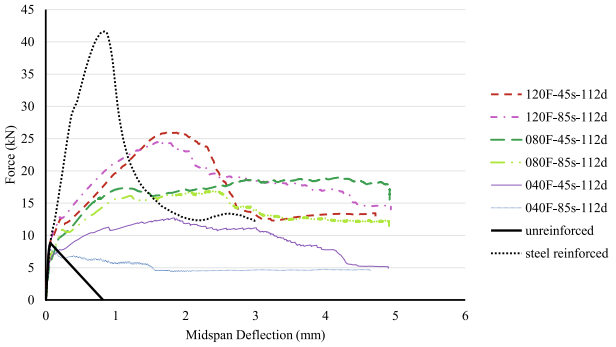

Fig. 3.6c. Flexural response of clamp enhanced OPBF reinforced concrete at 112 days.

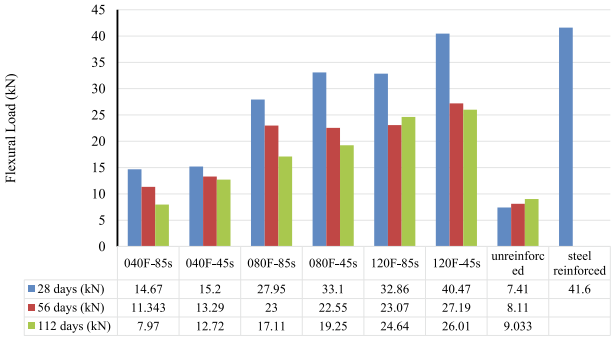

	040F-85s	040F-45s	080F-85s	080F-45s	120F-85s	120F-45s	unreinforced	steel reinforced
28 days (kN)	14.67	15.2	27.95	33.1	32.86	40.47	7.41	41.6
56 days (kN)	11.343	13.29	23	22.55	23.07	27.19	8.11	
112 days (kN)	7.97	12.72	17.11	19.25	24.64	26.01	9.033	

Fig. 3.7. Maximum flexural capacity of clamp enhanced OPBF reinforced concrete.

curve reduces. As the micro-cracks expand into macro-cracks and multiple macro-cracks develops, the slope continues to reduce until the maximum capacity (ultimate failure load) is reached. Then the force–deflection curve drops rapidly. Fig. 3.6 (a – c) present the results of the force–deflection curves at 28, 56 and 112 days respectively, while Fig. 3.7 presents the maximum flexural capacities of the samples. The flexural capacities of the samples increase with an increase in tendon area and reduced clamp spacing. The reduction of flexural capacities with age is due to the degradation of the OPBF-concrete interface. Alkali present in the cement embrittles and deteriorates the OPBF tendon surface thereby reducing the bond stress between reinforcement and matrix. This is common with fibres of vegetable origin [24].

Structural indicators such as pre-crack flexural stiffness, serviceability loads, post-cracking load, energy absorption and ultimate load-

Table 3.1
Structural indicators of unreinforced, OPBF reinforced and steel reinforced concrete beams.

Type of sample (reinforcement ratio %)	Structural indicators	OPBF-tendon reinforced concrete (maturity dates and clamp spacings)					
		28 days		56 days		112 days	
		45 mm	85 mm	45 mm	85 mm	45 mm	85 mm
Unreinforced concrete (0.00)	Pre-crack flexural stiffness (kN/mm)	**102.68**		**101.14**		**100.85**	
	Load at first crack (kN) / corresponding deflection (mm)	**7.085** /0.069		**7.687** /0.076		**8.068** /0.080	
	Ultimate load (kN) /corresponding deflection (mm)	**7.085** /0.069		**7.687** /0.076		**9.033** /0.095	
	Toughness kNmm	1.805		2.235		2.684	
40F (0.96)	Pre-crack flexural stiffness (kN/mm)	**146.98**	**156.10**	**133.06**	**161.68**	**127.36**	**172.25**
	Load at first crack (kN) /corresponding deflection (mm)	**7.780** /0.069	**7.760** /0.057	**7.700** /0.077	**7.862** /0.053	**6.80** /0.048	**7.97**/0.062
	Ultimate load (kN) /corresponding deflection (mm)	**14.60**/ 2.106	**14.34**/ 2.044	**13.29** /1.322	**11.34** /0.703	**12.72** /1.830	**7.97** /0.060
	Toughness kNmm	50.32	49.73	44.92	29.63	46.89	23.71
80F (2.33)	Pre-crack flexural stiffness (kN/mm)	**165.12**	**165.13**	**157.22**	**153.70**	**108.42**	**136.85**
	Load at first crack (kN) /corresponding deflection (mm)	**7.761** /0.051	**8.872** /0.113	**8.159** /0.067	**6.774** /0.055	**5.14** /0.049	**6.71** /0.066
	Ultimate load (kN) /corresponding deflection (mm)	**33.10** /3.157	**27.95** /2.567	**22.52** /1.993	**22.98** /1.367	**19.25** /3.96	**17.11** /2.40
	Toughness (kNmm)	117.60	97.18	76.55	67.05	82.37	67.23
120F (3.49)	Pre-crack flexural stiffness (kN/mm)	**129.51**	**130.52**	**130.22**	**165.45**	**166.86**	**168.60**
	Load at first crack (kN) /corresponding deflection (mm)	**5.764** /0.047	**8.751** /0.095	**8.143** /0.105	**7.005** /0.051	**8.87** /0.063	**8.15** /0.057
	Ultimate load (kN) /corresponding deflection (mm)	**40.20** /3.435	**32.50** /3.330	**27.18** /2.797	**23.04** /1.771	**26.01** /1.737	**24.64** /1.631
	Toughness (kNmm)	131.97	126.28	86.24	74.24	79.61	90.99
Steel- reinforced concrete (0.56)	Pre-crack flexural stiffness (kN/mm)	**149.21**					
	Load at first crack (kN) /corresponding deflection (mm)	**18.61** /0.217					
	Ultimate load (kN) /corresponding deflection (mm)	**41.6** /0.838					
	Toughness (kNmm)	59.77					

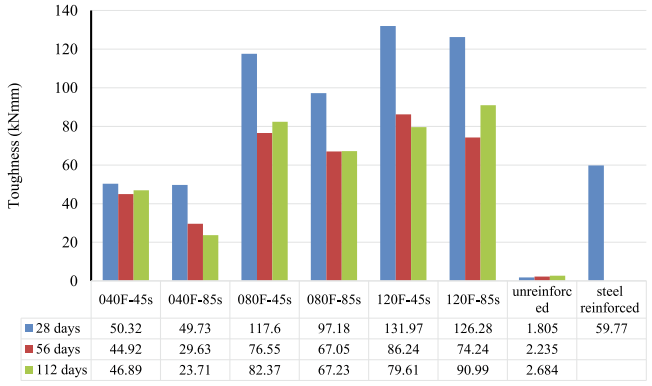

Fig. 3.8. Flexural toughness of clamp enhanced OPBF reinforced concrete at 28, 56 and 112 days.

to-weight ratios for the different tendon reinforcement areas, age of sample and clamp spacings are presented in Table 3.1.

There was no noticeable difference in pre-crack flexural stiffness of all the samples for all test durations though the load–deflection relationship was largely influenced by the reinforcement type. Compared with the steel reinforced sample, the OPBF tendon concrete generally experienced higher deflection (up to 5 mm) due to the relative lower stiffness of OPBF. The steel reinforced sample was characterised by sudden shear failure, hence the termination of the test at 3 mm deflection. However, for reinforcement ratios greater than 2.33%, the flexural response of the OPBF-tendon concrete displays better energy absorption which is usually one of the main characteristics of concrete reinforced with natural fibres [22]. The hose clamps acted like shear connectors by transferring tensile stresses from the concrete onto the tendons. Fig. 3.8 shows the calculated energy absorbed in flexural response (flexural toughness) by the samples. Energy absorbed was determined by using the trapezoidal rule to integrate the respective areas between the curve and the horizontal (midspan deflection) axis for each of the samples shown in Figs. 3.6 (a – c). The 120F-45 s-28d sample gives the highest value of energy absorbed (131.97 Joules) while the unreinforced sample gives the lowest absorbed energy (1.805 Joules).

Although the amount of energy absorbed was expected to reduce drastically with the age of samples due to the alkali-induced deterioration of the OPBF surface, only the 40F tendons seemed to meet this expectation. In fact, there were slight increases in energy absorption for the 80F and 120F tendons. This is because, for the 40F fibres the percentage of fibres forming the circumference of the tendons is greater than that for the 80F and 120F tendons. As the circumferential fibres absorbed moisture, although the bond with the concrete will soften, these fibres act as a protective layer to the inner fibres hence maintaining the strength of the inner fibres and enhancing the energy absorption of the composite. Generally, concrete reinforced with fibres of vegetative origin displays higher energy dissipation capacity than steel-reinforced concrete [7 15]. Crack development was noticed earlier for the tendon reinforced concrete due to factors such as microcracks development around hose clamps as a result of air bubbles trapped in the concrete during production, dimensional instability of the OPBF-tendons due to water absorption, degradation of tendon/concrete interface, and the relatively low modulus of elasticity of the tendons.

Unlike bamboo reinforced concrete, whose flexural response curve tends to be linear, OPBF-tendon concrete displays a 3-zone flexural response of elastic, elasto-plastic, and plastic, like steel reinforced concrete [20]. The tensile response of the individual tendons in which the fibres constituting the tendons fail gradually is responsible for this. This means that the mechanism of flexural response is governed by a complex combination of bond failure at concrete/tendon interface, failure of individual OPBF, mechanical interlocking of hose clamps in the concrete and damage of the concrete in tension and compression. The steel-reinforced concrete in this study failed in a sudden shear mode without yielding of the rebars due to the absence of shear reinforcement

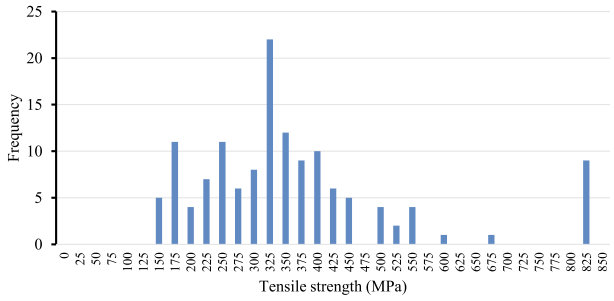

Fig. 3.9. Frequency distribution chart of tensile strength of OPBF obtained from 140 single fibres.

(stirrups). The shape of the force–deflection curve obtained for the steel-reinforced concrete (without stirrups) is consistent with the study of Kurumatani et al. [35].

The cracking moment (M_{cr}) can be determined directly from each curve at the point of appearance of the first crack. Due to the sudden drop in strength after cracking for the 40F tendons (see Figs. 3.6 a – c), minimum reinforcement ratio of 2.33% is recommended for OPBF reinforced concrete beams. From the flexural curves, it can be concluded that a reinforcement ratio of 3.49% (120F-45-28d) gives a commensurate performance with 0.56% of steel, in terms of the maximum flexural capacity of the beam section. The relatively low elastic modulus of natural fibres imply that a greater reinforcement ratio is needed for a comparative performance with steel reinforcement. This is corroborated in the studies of Muhtar et al. [20] who recommended 4% bamboo reinforcement ratio as an alternative to 0.89% steel for a 150x75x1000mm beam in flexure, and Agarwal et al. [12] who achieved a commensurate axial and lateral resistance for a 150x150x1000mm concrete column reinforced with 8% bamboo reinforcement instead of 0.89% of steel.

3.4. Practical design considerations

It is important to mention that the difference in the behaviour between conventional steel-reinforced concrete and OPBF-reinforced concrete leads to a different design approach. OPBF can be approximated as being elastic and brittle while steel can be ascertained as plastic and ductile. Therefore, a factored allowable strength for OPBF tendons needs to be adopted for a good margin of safety. Secondly, the relatively low bond strength at the tendon/concrete interface implies that the full strain-compatibility assumed between steel and concrete is not the case for the OPBF – tendon reinforced concrete. The lower elastic modulus of OPBF tendons (about 10% of steel) also implies that stringent design requirements may be necessary to satisfy serviceability.

Momoh et al. [23] carried out tensile strength test on single OPBF. Details of the test can be found in the study, however data from the study is plotted as a frequency distribution chart (and presented in Fig. 3.9). Characteristic tensile strength (f_{fT}) of 200 MPa can be adopted for a safe boundary due to the limited number of tensile tests carried out on the tendons (from Figs. 3.1 and 3.9). Using a material safety factor γ_{opbf} of 0.67, results in a tendon design strength (f_{fTd}) of 165 MPa and this leads to some practical design implications.

Other material properties determined from the experimental results in the present study are listed below:

- Concrete compressive strength, $f_{cu}^{'} = 40$ MPa
- Concrete modulus of rupture, $f_r = 3.4$ MPa
- OPBF tendon characteristic strength, $f_{fT} = 200$ MPa
- Design strength of OPBF (f_{fTd}) using a reduction factor of 0.67 = 165 MPa
- A 10 mm clear cover for all reinforcing members
- Beams are analysed as simply supported with four-point bending set-up.

The beam section is 100x100mm having various areas of OPBF reinforcements. The effective depth to the bottom reinforcement for the beam sections was determined as:

$d_x = 100 - 10(\text{cover}) - \varnothing/2$, (3.1).

where $\varnothing$ are the respective *diameters* of the OPBF tendon reinforcements. By using the Eurocode 2 [36] formula for determining the area of reinforcement required for a rectangular section, the maximum moment capacity of the section can be determined by:

$$M = 0.87 A f_{yd} z, \tag{3.2}$$

where A is the area of reinforcement, f_{yd} is the design strength of the steel reinforcement, and z is the lever arm of the section which usually has an upper limit of 95% of the effective depth (d_x). From Fig. 3.6a, the maximum flexural force (40kN) of the 120F-45 s-28d sample can be approximated to that of the control sample reinforced with 6 mm rebar (41kN). According to Eq. (3.2), the moment capacity of the control sample would be 2.03kNm assuming a yield stress of 500 MPa for the reinforcing steel. If we set the moment capacity of the section at 2.03kNm and replace the other terms of Eq. (3.2) with the corresponding quantities for the same section but reinforced with 120F OPBF tendons, a proportionate Eq. (3.2) for OPBF reinforced concrete would translate to Eq. (3.3) thus:

$$M = 0.46 A_f f_{fTd} z, \tag{3.3}$$

where A_f is the area of OPBF tendon reinforcement, f_{fTd} is the design strength of the OPBF tendon reinforcement, and z is the lever arm of the section taken as $0.95d$. From several measurements of tendon cross-sectional areas, a correlation between cross-sectional area (A_{tf}) and number of fibres (F) constituting a tendon was obtained as:

$F = A_t/1.456$ (3.4).

Equation 3.4 can be used to calculate the number of individual OPBF required for a calculated tendon area of reinforcement and vice versa. The accuracy of this correlation is 99.5% in terms of the coefficient of determination (R^2). Eq. (3.3) can be used to estimate the maximum moment capacity of an OPBF tendon reinforced section with hose clamps spaced at 45 mm. It also implies that the use of an equal area of OPBF tendons in place of steel rebar would result in about 55% reduction in the moment capacity of the section at serviceability limit state. In other words, a reinforcement ratio of 3.49% OPBF gives a commensurate performance with 0.56% of steel, in terms of the flexural capacity of the section. This trend of higher reinforcement area required for natural fibres can be seen in bamboo reinforced concrete beams with a reinforcement ratio of 4% bamboo against 0.89% steel [20]. Natural fibres due to their relatively low elastic modulus require a greater area of reinforcement in order to achieve a commensurate axial stiffness as reinforcement steel.

However, the relatively low modulus of elasticity of vegetative fibres causes excessive deflections when used as reinforcements in concrete [12] and this is no different for OPBF tendons. With OPBF tendon reinforcement deflection limits would be satisfied with a higher reinforcement ratio. Deflection checks for reinforced concrete beams are not carried out like in the case of steel sections, the serviceability of a reinforced concrete beam is measured by comparing the calculated span/effective depth ratio (L/d) with the limit specified in Eurocode 2 [36]. The span/effective depth ratio for the samples tested in this study satisfies the code requirement but the sample dimensions (100x100x500mm) may be too small to make recommendations especially on a new reinforcement type like OPBF tendons. However, considering the Eurocode 2 deflection limit of 0.4% span, the maximum deflection for a 450 mm span of 100x100mm (used in this study) would be 1.8 mm. From Figs. 3.6 (a – c), the steel-reinforced section clearly reaches its peak strength before the deflection limit while the OPBF-

tendons reinforced samples achieved only about 65% capacity at the deflection serviceability limit of 1.8 mm. The relatively high deflection at peak strength for the OPBF tendon reinforced samples would also create serviceability concerns such as unacceptable crack widths in practical application. The design implication is that the capacity of the section would be reduced, or the reinforcement ratio would need to be increased. In the case of increasing reinforcement ratio aggregate sizing of coarse aggregate would also be reduced to allow for adequate compaction during production. Further studies on creep of OPBF reinforced concrete would be revealing in terms of its long-term performance.

Another important consideration is the loss of bond due to alkali-induced embrittlement of the OPBF surface in the concrete matrix. Since most studies on bamboo reinforced concrete report on the mechanical behaviour at 28 days, findings on the long-term bond behaviour between bamboo and concrete is scarce thereby making the comparison of the results of this study difficult. Nonetheless, measures are required to mitigate the loss of bond at the concrete-OPBF interface in order to improve long term performance and further studies in this regard is necessary. Overall, the 28 days flexural performance of the OPBF tendon reinforced concrete is impressive. For an allowable stress design approach where the section is designed to perform within the elastic range, the tendons would serve satisfactorily as structural reinforcement for lintel beams. Therefore, the natural tendon reinforced concrete would be adequate for light structural members like lintel beams for residential housing. Furthermore, treatments such as surface coatings with adhesives which have proved successful for bamboo reinforcements [132155] can also be applied to OPBF tendons in order to enhance performance in the long term.

4. Finite element modelling of constituent materials

A popular method of modelling brittle materials is through the use of Concrete Damage Plasticity (CDP) concept which requires the formulation of a single constitutive model incorporating both tensile and compressive failures, with appropriate values of the relevant parameters [37 38]. CDP is based on two main damage criteria, i.e., tensile cracking and compressive crushing [39] while the failure surface is governed by the plastic strains in tension and compression. In other words, CDP predicts complete inelastic behaviour and damage of a material in both tension and compression. It has the advantage of being interpreted clearly with physical experimental parameters. Stress–strain response for the material under uniaxial compression is governed by a damage parameter d, specified with limits $0 < d < 1$. At full elasticity, $d = 0$ while at complete destruction, $d = 1$. In the absence of the damage parameter, the post-elastic response is fully plastic. This is because the CDP model is based on the response of concrete to triaxial stress. Setting $d_c = 0$ implies that the concrete is confined such that the confining force prevents crack propagation, thereby eliminating inherent brittleness and enhancing ductile behaviour [40]. The CDP concept, although originally developed for modelling concrete, has also found successful application in modelling other materials such as fibre-reinforced polymers [41] and has therefore been used for modelling the behaviour of tendons in this study. ABAQUS/Standard and ABAQUS/Explicit were employed in the modelling of plain concrete and OPBF tendon reinforced concrete respectively.

4.1. Modelling of plain concrete

4.1.1. Behaviour of concrete in compression

Modelling concrete behaviour in ABAQUS requires the user to specify the following:

Compressive stresses (f_c)
Inelastic strains (ε^{in})
Compressive damage parameter (d)

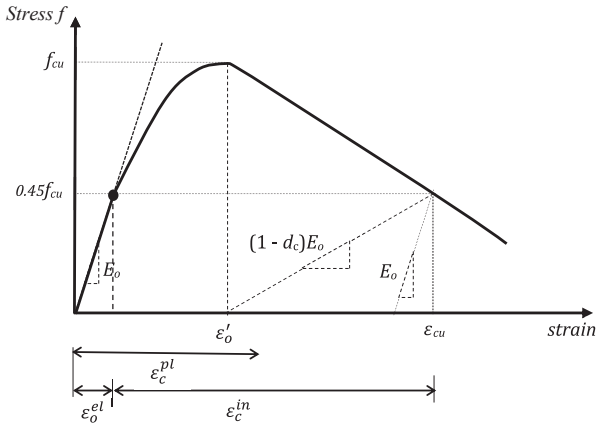

Fig. 4.1. Simplified analytical stress–strain curve for concrete under uniaxial compression.

The maximum uniaxial compressive strength for unconfined concrete was obtained from compressive strength test and was used to develop the stress–strain data used as input for ABAQUS. The constitutive model employed is the popularly used Ritter's parabola as explained in the study of Hognestad [42 43]. Using the Ritter's parabola, the ascending part of the uniaxial stress–strain relationship of concrete was defined by Eq. (4.1) and the softening part simplified by a constant slope as shown in Eq. (4.2).

$$for 0 < \varepsilon < \varepsilon_o^{'} : \frac{f}{f_{cu}} = 2\frac{\varepsilon}{\varepsilon_o^{'}}\left(1 - \frac{\varepsilon}{\varepsilon_o^{'}}\right) \tag{4.1}$$

$$for \varepsilon_o^{'} < \varepsilon < \varepsilon_{cu} : \frac{f}{f_{cu}} = 1 - 0.15\left(\frac{\varepsilon - \varepsilon_o^{'}}{\varepsilon_{cu} - \varepsilon_o^{'}}\right), \tag{4.2}$$

where f_{cu} is the maximum uniaxial compressive strength and ε is strain, ε_{cu} is the corresponding maximum strain.

Without experimental data, it is possible to obtain stress–strain data for normal strength concrete using Eqs (4.1) and (4.2) and strain at maximum stress $\varepsilon_o^{'}$ from Eq. (4.3) [44]:

$$\varepsilon_o^{'} = (0.71 f_{cu} + 168)\text{x } 10^{-5} \tag{4.3}$$

The inelastic strain ε^{in} is defined as the strain beyond which the concrete changes from elastic response to inelastic response. Studies recommend using 40–50% of the peak compressive strength (f_{cu}) at the maximum elastic strain for concrete [43 45 46], hence a value of 45% has been used in this study. The commencement of inelastic response is illustrated in the stress–strain curve shown in Fig. 4.1. The total strain tensor ε_{cu} is the sum of the elastic strain ε_o^{el} and the inelastic strain ε^{in} as defined in Eq. (4.4):

$$\varepsilon_{cu} = \varepsilon_o^{el} + \varepsilon^{in} \tag{4.4}$$

where.

$$\varepsilon_o^{el} = \frac{f_c}{E_0} \tag{4.5a}$$

which could be re-written as.

$$f_c = E_o\left(\varepsilon_{cu} - \varepsilon^{in}\right) \tag{4.5b}$$

The relationship between the compression damage parameter d_c, and the elastic stiffness E_0 can be written thus:

$$E = (1 - d_c)E_o, \tag{4.5c}$$

where E_o and E are the undamaged elastic stiffness and the post-elastic stiffness of the concrete respectively.

A simplified relationship between stress at any given point (f_c)

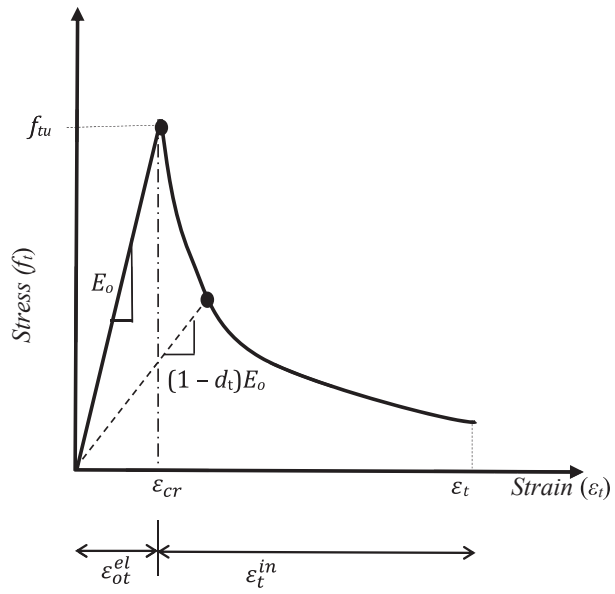

Fig. 4.2. Simplified analytical stress–strain curve for concrete under uniaxial compression.

beyond the maximum stress (f_{cu}) and damage parameter (d_c) is therefore given as:

$$d_c = 1 - \frac{f_c}{f_{cu}} \tag{4.6}$$

Combining Eqs 4.5a, 4.5b and 4.6 gives the uniaxial compression response of concrete with respect to the CDP model (Eq. (4.7)):

$$f_c = \frac{\varepsilon_{cu} - \varepsilon^{in}}{1 - d_c} E \tag{4.7}$$

Similarly, the maximum uniaxial compressive stress can be written as.

$$f_{cu} = \frac{f_c}{(1 - d_c)} \equiv E_o\left(\varepsilon_{cu} - \varepsilon^{in}\right) \tag{4.8}$$

An average compressive strength of 40 MPa was obtained from the compressive strength test of 100 mm cubic samples while Elastic modulus E_o of 35.5GPa was selected for the 40 MPa concrete with guidance from Eurocode 2 [36]. These were used as inputs to generate the stress–strain data of the concrete in compression (see Table 4.1).

4.1.2. Behaviour of concrete in tension

Like compression modelling, concrete tensile behaviour in ABAQUS requires the user to specify the following:

Tensile stresses (f_t)
Inelastic strains (ε^{in})
Tensile damage parameter (d_t)

Reliable behaviour in tension is difficult to obtain by subjecting concrete to direct tension, hence splitting tensile tests were performed as an indirect procedure for measuring concrete tensile behaviour. For the purpose of modelling, mean tensile strength (f_{ctm}) can be derived analytically using Eq. 4.9a which shows that the mean tensile strength for normal strength concrete is about 10–12% of the characteristic compressive strength of a cylindrical concrete specimen (f_{ck}). For concrete strength classes above C50/60, f_{ctm} is derived from the mean compressive strength (f_{cm}) and the relationship is shown in Eq. 4.9b [47]:

$$f_{tm} = 0.30\left(f_{ck}^{2/3}\right) \tag{4.9a}$$

$$f_{tm} = 212 log_e\left[1 + \frac{f_{cm}}{10}\right] \tag{4.9b}$$

Similar to the compressive stress–strain curve, the tensile stress–-strain curve is divided into the linear elastic ascending part and the post-failure tension softening response. Post-peak tension softening can be modelled in three ways: linear, bilinear, or exponential [45]. In this study, the exponential softening response best described the results of the split tensile test conducted and was hence adopted such that:

$$for \varepsilon_t \le \varepsilon_{cr} : f_t = E_o \varepsilon_t \tag{4.10a}$$

$$for \varepsilon_t \ge \varepsilon_{cr} : \frac{f_t}{f_{tu}} = \left(\frac{\varepsilon_{cr}}{\varepsilon_t}\right)^n, \tag{4.10b}$$

where ε_t is the tensile strain at any point on the stress–strain strain curve (see Fig. 4.2), ε_{cr} is the cracking strain and n is a parameter which is used to calibrate the post-yield response of the stress–strain curve to fit experimental data. Typical range for n is 0.4 – 1.5 [47]. In this study, n = 0.4 was adopted. The maximum tensile strength (f_t) of 3.45 MPa was obtained from the split-tensile strength test carried out on the 100∅x200mm plain concrete cylinder samples and has been used to generate the stress–strain data of the concrete in tension (see Table 4.1).

For both compression and tension, post-peak stress damage was defined using Eq. (4.6) and (4.12), respectively. The tension damage parameter has the range $0 < d_t < 1$ where *0* represents undamaged state while *1* represents complete destruction in tension. Fig. 4.3a and 4.3b

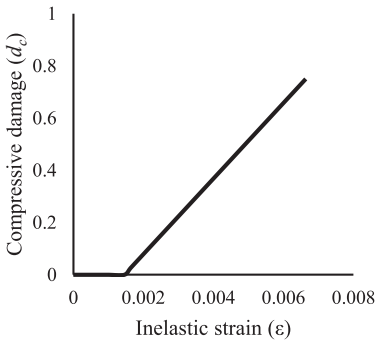

(a) Compressive damage curve

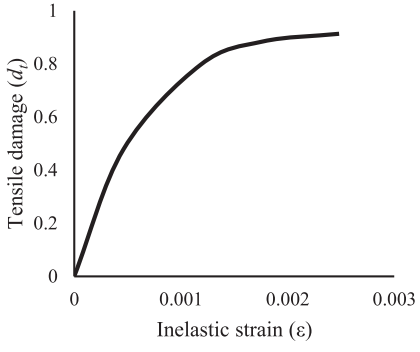

(b) Tension damage curve

Fig. 4.3. Damage curves for the concrete.

Table 4.1
Stress–strain and damage data input in ABAQUS for concrete.

Compression			Tension		
Compressive stress f_c (MPa)	Inelastic strain ϵ^{in} (Eq. (4.4))	Damage parameter d_c (Eq. (4.6))	Tensile stress f_c (MPa)	Inelastic strain ϵ_t^{in}	Damage parameter d_t
18	0	0	3.45	0	0
22	0.00013905	0	1.8	0.000456	0.478
26	0.000294623	0	0.7	0.001181	0.797
28	0.000380814	0	0.4	0.001762	0.884
30	0.000474542	0	0.3	0.002477	0.913
32	0.000578215	0			
34	0.000695889	0			
36	0.000835469	0			
38	0.001017379	0			
40	0.00145654	0			
39	0.001629207	0.025			
38	0.001801874	0.05			
34	0.00249254	0.15			
30	0.003183207	0.25			
26	0.003873874	0.35			
22	0.004564549	0.45			
18	0.005255216	0.55			
14	0.005945874	0.65			
10	0.00663654	0.75			

show the damage curves for the data input in ABAQUS.

Similar to the compression response, the uniaxial tension response of concrete with respect to the CDP model is given as:

$$f_t = \frac{\varepsilon_t - \varepsilon^{in}}{1 - d_t} E \tag{4.11}$$

$$f_{tu} = \frac{f_t}{(1 - d_t)} = E_o\left(\varepsilon_t - \varepsilon^{in}\right) \tag{4.12}$$

The uniaxial compression and tension data entered into ABAQUS is the compressive/tensile stress *versus* inelastic strain data: i.e $f_c - \varepsilon_c^{in}$ and $f_t - \varepsilon_t^{in}$ curves. Inelastic strain is the difference between maximum elastic strain and the total strain for each regime. In other words, the stress–-strain data fed into ABAQUS are the "f_c *versus* $(\varepsilon_{cu} - \varepsilon_o^{el})$ and f_t *versus* $(\varepsilon_t - \varepsilon_{ot}^{el})$" curves for the compressive and tensile material properties respectively. ABAQUS software calculates the plastic strain (ε^{pl}) using Eq. (4.13):

$$\varepsilon^{pl} = \varepsilon^{in} - \frac{d_t}{1 - d_t}, \tag{4.13}$$

where d and f are the respective damage parameter and stress respectively. It is important to check that the plastic strain is positive and ascending in magnitude in both damage regimes. In the case that it is negative or descending in magnitude, it would be impossible to calculate the damage in the material. The implication is that the unloading path intersects with the loading path and hence damage does not exist [48].

Table 4.1 show the stress–strain and damage input data for concrete in compression and tension in ABAQUS.

4.1.2.1. Parameters and solution procedure. CDP requires some physical parameters for defining material behaviour. These include eccentricity (ϵ), dilation angle (ψ), and stiffness recovery factor.

Eccentricity (ϵ) is set to a default value of 0.1 which implies that ψ is the same for a wide range of confining pressures [45]. Another parameter governing the CDP behaviour of concrete is f_{bo}/f_{co} which is the ratio of concrete strength in biaxial compression (f_{bo}) to its strength in uniaxial compression (f_{co}). Recommendation for f_{bo}/f_{co} is given in the study of Kupler such that $f_{b0} = 1.16248\, f_{co}$ [49]. ABAQUS uses a default value of 1.16 which has been employed in this study.

Table 4.2
Material properties of concrete.

Property	Value	Reference
Density	2340 kg/m^3	This study
Young's Modulus E	35.5 GPa	[36]
Poisson ratio	0.15	[52]
Dilation angle ψ	35	
Eccentricity ϵ	0.1	
f_{bo}/f_{co}	1.16	
K	0.67	
Viscosity Parameter	0	

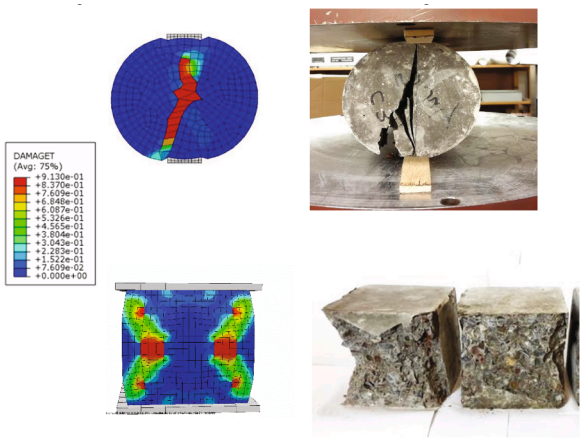

Fig. 4.4. Comparison of damage (crack) of plain concrete between FE-model and experimental sample.

Dilation angle (ψ) is interpreted as the internal friction angle of concrete which is reported to be between 20^0 and 40^0 [45]. Technically, it is the angle subtended by the failure surface with the hydrostatic axis and measured in the meridional plane. Accurate prediction of post-cracking behaviour of concrete requires combined tension and shear experiments which are difficult to carry out. In the absence of such data, it can be assumed that the shear retention factor goes linearly to zero at the same crack opening strain adopted for tension stiffening [50]. A ψ value of 35^0 has been adopted in this study.

Stiffness recovery is expressed in the percentage of the undamaged stiffness and is more useful for cyclic loading [51]. It is assumed that compressive stiffness is fully recovered upon crack closure as the loading changes from tension to compression. Contrarily, tensile stiffness is lost as the load changes from compression to tension. Hence a default value of compressive stiffness reduction factor of 1 is assumed while tensile stiffness reduction factor is 0. Furthermore, a zero-tension stiffness recovery implies that material tangential to the tension plane is affected by the damages in compression.

Material properties and parameters of concrete used in the model are shown in Table 4.2.

Concrete was discretized using 8-noded-brick elements with reduced integration (CD8R). The calibration of the concrete models was performed using the Static, General (Full Newton) procedure while the tendon reinforced concrete models were analysed using quasi-static (dynamic, explicit) procedure. Dynamic Explicit was chosen for the modelling of the clamp-enhanced tendon reinforced concrete due to the complexity of the contact definitions which are difficult to simulate using static analysis procedure. The quasi-static approach is also more efficient in calculating deformation because it performs direct-integration using the central-difference operator to match in pseudo-time. Hence care should be taken concerning inertial effects that could lead to unstable material behaviour. However, unstable responses can be reduced by reducing the loading rate or by increasing the mass density

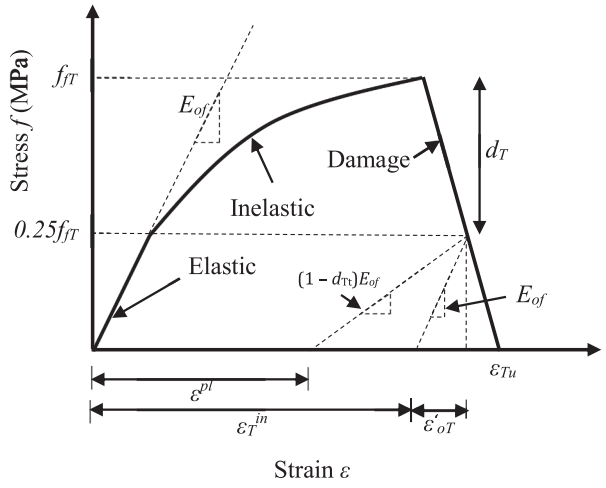

Fig. 4.5. Simplified tensile stress–strain curve for OPBF tendons enhanced with steel clamps.

[53].

For the static analysis of the plain concrete samples, the time-period was set to 0.001, the maximum number of increments to 10,000 and the minimum set to 1E-50. ABAQUS requires that the first pair of data for both compression and tension correspond to the onset of inelastic behaviour by the material. Displacement control strategy was employed by applying a known displacement to the point of application of the load in the model. Fig. 4.4 shows good agreement in crack patterns between experiments and finite element model of the plain concrete. Hence the selected CDP parameters are adequate for the material definition of plain concrete and were employed in the modelling of the tendon-reinforced concrete.

4.2. Modelling of OPBF tendons

4.2.1. Behaviour of OPBF in tension

The uniaxial stress–strain relationship for OPBF tendons derived from experiments was then used as input in ABAQUS. This was achieved by using simplified stress–strain relationship to formulate the constitutive equations. It is shown that the stress–strain relationship of OPBF tendons is characterised by three regimes: the ascending (elastic) part, the inelastic part, and the descending part as illustrated in Fig. 4.5.

Using the concept of CDP, the uniaxial stress–strain relationship of the tendons can be defined by Eqs 4.14–4.16:

$$for 0 < \varepsilon < \varepsilon'_{oT} : f_f = E_{of}\varepsilon \tag{4.14}$$

$$\varepsilon'_{oT} < \varepsilon < \varepsilon_T : f_f = \alpha\varepsilon^2 + \beta\varepsilon + \gamma \tag{4.15}$$

$$\varepsilon_T < \varepsilon < \varepsilon_{Tu} : f_f = \lambda_1\varepsilon + \lambda_2 \tag{4.16}$$

where f_{fT} is the maximum uniaxial tensile strength, ε_T is the corresponding strain and α, β, γ, λ_1 and.

λ_2 are constants. The inelastic strain ε_T^{in} is defined as the strain beyond which the tendon changes from elastic response to inelastic response. Experimental data show that the onset of inelastic strain is at about 25% of the maximum tensile strength (f_{fT}). The total strain tensor ε_{Tf} is the sum of the elastic strain ε_{of}^{el} and the inelastic strain $\varepsilon_f{}^{in}$ as defined in Eq. (4.17):

$$\varepsilon_{Tf} = \varepsilon_{of}^{el} + \varepsilon_f^{in} \tag{4.17}$$

$$\varepsilon_{of}^{el} = \frac{f_f}{E_{of}} \tag{4.18}$$

which could be re-written as.

$$f_f = E_{of}\left(\varepsilon_{Tu} - \varepsilon_T^{in}\right) \tag{4.19}$$

Such that a tension damage parameter d_{Tf}, defines stiffness degradation as:

$$E = \left(1 - d_{Tf}\right)E_{of} \tag{4.20}$$

where E_{of} and E_f are the undamaged elastic stiffness and the post-

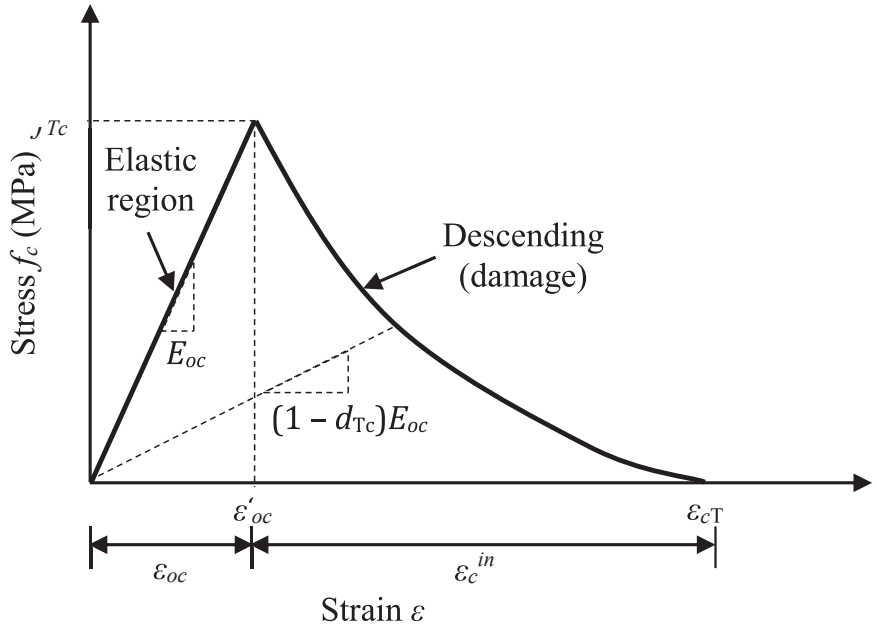

Fig. 4.6. Simplified compressive stress–strain curve for OPBF tendons enhanced with steel clamps.

Table 4.3
CDP material parameters for OPBF tendons.

Property	Value	Reference
Density	840 kg/m^3	[24]
Young's Modulus E_{oT}	26.6GPa	This study
Poisson ratio	0.4	This study
Dilation angle ψ	35^0	[52]
Eccentricity ϵ	0.1	[52]
f_{bo}/f_{co}	1.16	[52]
K	0.67	[52]
α	-1.9×10^5	This study
β	1.2×10^4	This study
γ	34.47	This study
α_c	0.0938	This study
β_c	−1.064	This study
λ_1	-2.5×10^4	This study
λ_2	698.87	This study

elastic stiffness of the OPBF tendon respectively.

Similar to the modelling approach for concrete, a simplified relationship between stress at any given point (f_f) beyond the maximum stress (f_{fT}) and damage parameter (d_{Tf}) is therefore given as:

$$d_{Tf} = 1 - \frac{f_f}{f_{fT}} \tag{4.21}$$

And the plastic strain is calculated using Eq. (4.22):

$$\varepsilon_T^{pl} = \varepsilon^{in} - \frac{d_{Tf}}{1 - d_{Tf}} \left(\frac{f_f}{E_{of}} \right) \tag{4.22}$$

4.2.2. Behaviour of OPBF in compression

For modelling, the stress – strain relationship of OPBF tendons in compression was simplified into two regimes: the ascending (elastic) part and the descending/strain hardening (damage) part (see Fig. 4.6). The uniaxial compressive stress–strain relationship of the tendons can be defined by Eqs (4.23) and (4.24):

$$for 0 < \varepsilon < \varepsilon_{oc}^{'} : f_{fc} = E_{of}\varepsilon \tag{4.23}$$

$$\varepsilon_{oT}^{'} < \varepsilon < \varepsilon_{cT} : f_{fc} = \alpha_c e^{\beta_c} \tag{4.24}$$

Like the OPBF tendon in tension, the inelastic strain ε_c^{in} is defined as the strain beyond which the tendon changes from elastic response to inelastic response under compression. Experimental data show that the onset of inelastic strain is at compressive strength (f_{fc}) of about 20 MPa for the 45 mm spaced clamps and between 4.8 and 7 MPa for the 85 mm spaced clamps. However, for a tendon in concrete, the surrounding concrete would provide confinement such that the confined compressive strength of the tendons would be higher. The total strain tensor ε_{cT} is the sum of the elastic strain ε_{oc}^{el} and the inelastic strain ε_c^{in} as defined in Eq. (4.25) (and shown in Fig. 4.6):

$$\varepsilon_{cT} = \varepsilon_{oc}^{el} + \varepsilon_c^{in} \tag{4.25}$$

$$\varepsilon_{oc}^{el} = \frac{f_{cT}}{E_{of}} \tag{4.26}$$

which could be re-written as:

$$f = E_{of}\left(\varepsilon_{cT} - \varepsilon_c^{in}\right) \tag{4.27}$$

Such that a compressive damage parameter d_{Tc}, defines stiffness degradation as:

$$E_{fc} = (1 - d_{cT})E_{of} \tag{4.28}$$

where E_{of} and E_{fc} are the undamaged elastic stiffness and the post-elastic stiffness of the OPBF tendon in compression respectively.

Similar to the modelling approach for concrete, a simplified relationship between stress at any given point (f_f) beyond the maximum stress (f_{fc}) and damage parameter (d_{cT}) is therefore given as:

Table 4.4
Stress–strain data in tension and compression for OPBF tendons.

Tension Stress MPa	Inelastic strain	Damage	Compression Stress MPa	Inelastic strain	Damage
65	0	0	65	0	0
70	0.000433	0	50	0.000188	0.230769
75	0.000924	0	40	0.000752	0.384615
80	0.001422	0	30	0.001881	0.538462
85	0.001928	0	20	0.003573	0.692308
90	0.002442	0	10	0.01072	0.846154
95	0.002966	0			
100	0.003498	0			
105	0.004041	0			
110	0.004593	0			
115	0.005157	0			
120	0.005733	0			
125	0.00632	0			
130	0.006922	0			
135	0.007537	0			
140	0.008168	0			
145	0.008815	0			
150	0.00948	0			
155	0.010164	0			
160	0.01087	0			
165	0.011599	0			
170	0.012354	0			
175	0.013137	0			
180	0.013953	0			
185	0.014805	0			
190	0.0157	0			
195	0.016644	0			
200	0.017645	0			
180	0.0185	0.1			
170	0.019	0.15			
160	0.0195	0.2			
150	0.02	0.25			
140	0.0205	0.3			
130	0.021	0.35			
120	0.0215	0.4			
110	0.022	0.45			
100	0.0225	0.5			
90	0.023	0.55			
80	0.0235	0.6			
70	0.024	0.65			
60	0.0245	0.7			
50	0.025	0.75			
40	0.0255	0.8			
30	0.026	0.85			

$$d_{cT} = 1 - \frac{f_f}{f_{fc}} \tag{4.29}$$

Similarly, the plastic strain is calculated using Eq. (4.30):

$$\varepsilon^{pl} = \varepsilon^{in} - \frac{d_{cT}}{1 - d_{cT}} \left(\frac{f_f}{E_{of}} \right) \tag{4.30}$$

The OPBF tendon reinforcement was also modelled using CD8R deformable homogeneous elements. Interaction between the concrete reinforcement was defined as surface-to-surface contact while the interaction property was defined as cohesive. Material parameters and stress–strain data in tension and compression for the tendons used as input in ABAQUS for the model are shown in Table 4.3 and Table 4.4 respectively. For the purpose of simplicity in modelling, the same CDP parameters used for the concrete were used since the OPBF would be fully confined in the concrete. For the 20 MPa compressive strength derived from the experiment, however, the finite element solution procedure of the tendon-reinforced concrete runs into error since the rate of deformation exceeds the rate of propagation of the stress waves in the OPBF elements. Although the actual value of the increase in compressive strength (and by implication the dilation angle) due to the confinement is difficult to determine, it was found that a range of

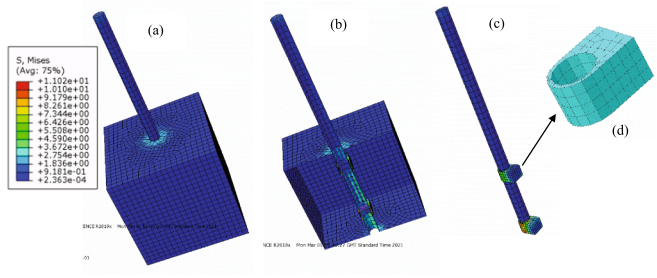

Fig. 4.7. Stress distribution in bond pull-out model (a) bond pull out model (b) cut-through section of model (c) OPBF tendon fitted with clamp (d) clamp.

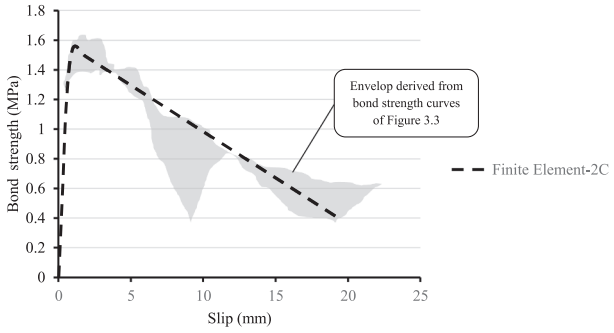

Fig. 4.8a. Bond pull-out envelop for 2 embedded clamps with finite element solution.

28–50% of compressive-to-tensile strength ratio sufficed. Hence 65 MPa compressive strength was used for the OPBF confined in concrete for this study.

4.3. Finite element modelling of bond pull-out

The bond between OPBF and concrete was modelled in ABAQUS using surface-based cohesive contact modelling. Factors which informed the use of this approach include the relatively weak interface between the OPBF and the concrete as compared to their individual material properties and the negligible thickness of the interface. Furthermore, the selected approach requires no need for defining an initial crack to simulate the progression of damage like in classical fracture mechanics [54 55]. Cohesive contact modelling possesses reduced mesh sensitivity and does not depend on the mass of the two surfaces in contact, hence reducing computational efforts [56]. The appropriateness of surface-based cohesive contact modelling for simulating bond pull-out behaviour of cementitious composites [57 58], and flexural behaviour of reinforced concrete [35 53 59] is well established.

Concrete, OPBF-tendons, and hose clamps were modelled using eight-node linear brick elements with reduced integration (C3D8R). A circular cross-section was assumed for the OPBF-tendons while the clamps were simplified to circular rings with rectangular projection (see Fig. 4.7). All other dimensions in the models are consistent with the physical dimensions from the experiments. Hard contact was defined in the normal direction between the tendons and the clamps to avoid surface penetration problems in the model. Each concrete block was modelled with a hole whose diameter is the same as that of the tendon to be inserted. The tendon was inserted to the 80 mm embedded length. The hole in the concrete model was assigned as the master surface while the surface of the tendon was assigned the slave surface. The clamps were then constrained as an embedded region with the concrete as the host region. The boundary conditions include applying an "encastre" over the concrete and applying a displacement of 25 mm (out of and

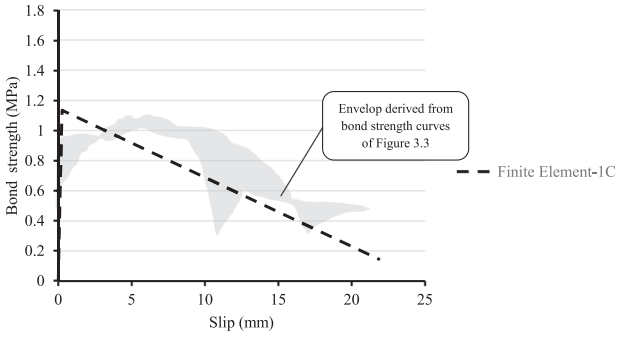

Fig. 4.8b. Bond pull-out envelop for 1 embedded clamp with finite element solution.

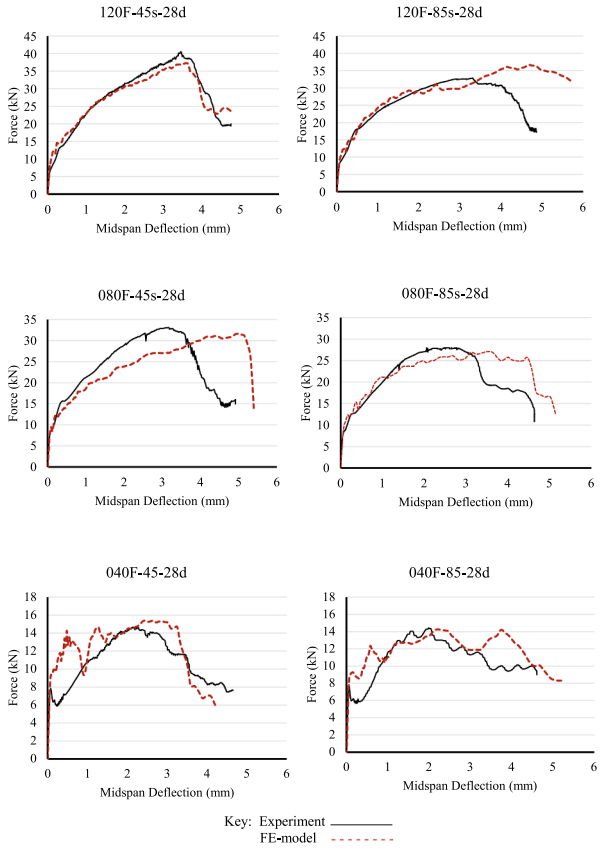

Fig. 4.9. Comparison between the experimental flexural response of the OPBF tendon reinforced beams and the 3D FE-models.

normal to the concrete) onto the end of the tendon.

The 25 mm pull-out distance is consistent with the pull-out distance in the experiment. A mesh size of 10 mm, 5 mm and 2.5 mm was used for the concrete, tendon and clamp respectively. A detailed theory explaining the constitutive relationship of the contact between OPBF, and concrete can be found in an earlier study by the authors [24].

Fig. 4.7 reveals that the stress in the concrete as a result of tendon pull-out was minimum. This corroborates the experimental observation that the tendons pull out of the concrete without visible damage to the concrete. Two models were developed and analysed to describe the average bond response of single embedded and double embedded clamps in the concrete. The bilinear response is plotted on the respective experimental bond pull-out envelops in Fig. 4.8a and 4.8b. The envelops

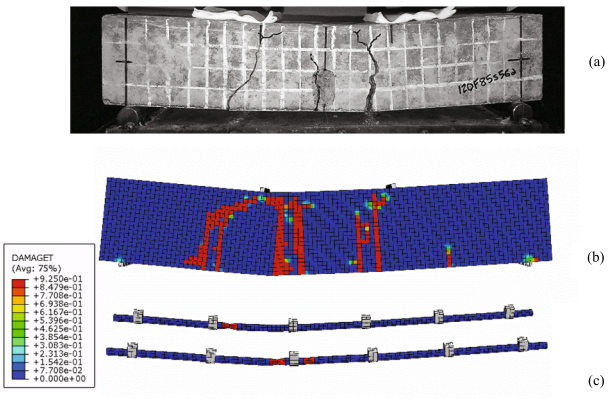

Fig. 4.10. (a) Flexural sample after test (b) Tensile damage in FE-model of concrete (c) Tensile damage in FE-model of OPBF tendon.

are the boundaries of the bond pull-out curves of Fig. 3.3. The cohesive surface modelling is therefore also applied in simulating the flexural behaviour of the OPBF-tendon reinforced concrete.

4.4. Modelling of OPBF tendon reinforced concrete

The OPBF tendon reinforcement was also modelled using C3D8R deformable homogeneous elements. Interaction between the concrete reinforcement was defined as surface-to-surface contact while the interaction property between them was defined as cohesive. Refer to Tables 4.4 for material properties of the tendons used in the model. The hose clamps were modelled as a perfectly plastic mild steel with a yield strength of 350 MPa and a modulus of elasticity of 200GPa. Due to the torque applied by the hose clamps onto the tendons, it is assumed that the relative slip between clamp and tendon is negligible. Hence a "tie" constraint was defined between the clamps and tendons, while cohesive surface modelling was used to define the interaction between the tendons and the concrete. ABAQUS approximates the relationship between cohesive stiffness in the normal direction (k_{nn}) and in the shear (k_{ss}) and tangential (k_{tt}) directions as shown in Eqs (4.31) – (4.32) [53]:

$$k_{nn} = 100k_{tt} = 100k_{ss} \tag{4.31}$$

$$k_{ss} = k_{tt} = \frac{\sigma_{max}}{\delta}, \tag{4.32}$$

where σ_{max} is bond strength between tendon and host matrix and δ is the slip at maximum bond stress.

Fig. 4.9 presents a comparison between the experimental flexural response of the OPBF-tendon reinforced beams with the 3D FE-models. There is good agreement between the force–deflection curves of the experiments and the FE models. The tensile damage pattern of the FE-models also shows good agreement with the crack pattern of the experimental samples (see Fig. 4.10). Table 4.5 presents a comparison between the experimental flexural responses and the finite element models in terms of ultimate and serviceability limit states of strength and deflection, respectively.

The difference between the experimental and finite element flexural capacity of the 040F-45 s-28d and 080F-45 s-28d samples at serviceability limit state seems to be quite high. This is due to the inherent variability in properties of natural fibres even of the same species which is a major concern when dealing with natural fibres. This is due to the functional grading of plant tissues to resist environmental forces such as wind. These variations in physical and mechanical properties exists even among fibres from the same oil palm species [23 60]. Therefore, modelling the behaviour of this type of material already presents several challenges. Furthermore, deflections at peak stress for the finite element models are slightly higher than that of the experimental samples. This may be due to the selection of a high dilation angle for the OPBF which assumed that the OPBF reinforcement are highly confined in the concrete and hence delaying the damage regime of the reinforcement. There could also be other reasons such as the simplification of the bond behaviour between the OPBF reinforcement and concrete to a bilinear regime (shown in Fig. 4.8(a) and 4.8 (b)). An in-depth investigation into these finite element parameters is however outside the scope of this study and has been noted for further investigation. Nevertheless, there is a good agreement in the values of maximum flexural capacities and that indicates that the experimental results support the findings of the FE-models.

5. Conclusions

This study focused on assessing the behaviour of OPBF-tendon reinforced concrete. Although only little is known about the prospects of OPBF as longitudinal reinforcement for structural members, the study has attempted to assess bond pull-out strength and flexural capacities of concrete reinforced with the natural fibres in the form of tendons actualised by hose clamps. Finite element modelling has also been carried out. Consequently, the following key findings are highlighted:

- A beam section reinforcement ratio of 3.49% OPBF tendon gives a commensurate performance to 0.56% of steel in terms of flexural capacity at 28 days,

Table 4.5
Comparison between flexural capacities between experimental and finite element models.

Sample ID	Maximum Flexural Capacity (kN) (Ultimate Limit State)		% Difference (Ultimate Limit State)	Flexural Capacity (Serviceability Limit State)		% Difference (Serviceability Limit State i.e., at 1.8 mm deflection)
	Experiment	**Finite Element Model**		**Experiment**	**Finite Element Model**	
Control	7.085	6.960	1.8	NA	NA	NA
040F-45 s-28d	14.60	15.37	5.3	14.03	13.80	1.6
040F-85 s-28d	14.34	14.26	0.6	13.40	13.00	3.0
080F-45 s-28d	33.10	31.93	3.5	27.60	23.47	15.0
080F-85 s-28d	27.95	27.10	3.0	26.47	24.42	7.7
120F-45 s-28d	40.20	37.56	6.6	30.07	29.48	2.0
120F-85 s-28d	32.50	36.40	12.0	28.35	28.62	1.0

- Bond strength of up to 1.6 MPa was achieved at 28 days, with average reductions in bond strength of 14% and 27% recorded at 56 days and 112 days respectively,
- Reduction in bond strength is responsible for the reduction in the flexural capacity of the OPBF-tendon reinforced concrete and this is due to the alkali deterioration of the tendon surface/concrete interface.
- A minimum reinforcement ratio of 2.33 is recommended for OPBF tendon reinforced concrete,
- OPBF-tendon reinforced concrete can be modelled using the concrete damage plasticity approach and the interaction between concrete and OPBF tendons can be accurately predicted using cohesive contact modelling,
- OPBF-tendon reinforced concrete can be used for light structural members such as lintels in residential housing.
- Surface treatment by adhesive coating is recommended for OPBF to preserve the concrete/reinforcement interface and maintain bond strength,
- Finally, the excessive deflection of OPBF tendon reinforced concrete indicates stringent serviceability requirements in the design of flexural elements.

CRediT authorship contribution statement

Emmanuel Owoichoechi Momoh: Funding acquisition, Conceptualization, Methodology, Investigation, Data curation, Formal analysis, Visualization, Resources, Writing – original draft, Writing – review & editing. **Adelaja Israel Osofero:** Funding acquisition, Project administration, Conceptualization, Supervision, Methodology, Writing – review & editing. **Oleksandr Menshykov:** Investigation, Supervision, Writing – review & editing.

Declaration of Competing Interest

The authors declare that they have no known competing financial interests or personal relationships that could have appeared to influence the work reported in this paper.

Acknowledgement

The authors wish to thank the Petroleum Technology Development Fund (PTDF) of Nigeria for sponsoring this study.

References

[1] E.-h. M. Bah, I. Faye and Z. F. Geh, The Housing Sector in Africa: Setting the Scene. In: Housing Market Dynamics in Africa, London: Palgrave Macmillan, 2018.
[2] BMU, "Sustainable buildings and construction in Africa," Federal Ministry for the Environment, Nature Conservation and Nuclear Safety, Bonn, Germany, 2016.
[3] E.A. Moore, Addressing housing deficit in Nigeria: issues, challenges and prospects, Economic and Financial Review (December 2020) 201–222.
[4] A.M. Auerbach, T. Thachil, How does Covid-19 affect urban slums? Evidence from settlement leaders in India, World Development 140 (2021), 105304.
[5] V. Sharma, B.M. Marwaha, H.K. Vinayak, Enhancing durability of adobe by natural reinforcement for propagating sustainable mud housing, International Journal of Sustainable Built Environment 5 (1) (2016) 141–155.
[6] M. Machaka, H. Basha, H.A. Chakra, A. Elkordi, Alkali treatment of fan palm natural fibers for use in fiber reinforced concrete, European Scientific Journal 10 (12) (2014) 186–195.
[7] L.C. Roma, L.S. Martello, H. Savastano, Evaluation of mechanical, physical and thermal performance of cement-based tiles reinforced with vegetable fibers, Construction and Building Materials 22 (4) (2008) 668–674.
[8] H. Savastano, V. Agopyan, A.M. Nolasco, L. Pimentel, Plant fibre reinforced cement components for roofing, Construction and Building Materials 13 (8) (1999) 433–438.
[9] F. Asdrubali, F. D'Alessandro, S. Schiavoni, A review of unconventional sustainable building insulation materials, Sustainable Materials and Technologies 4 (2015) 1–17.
[10] W. Wang, M. Sain, P.A. Cooper, Study of moisture absorption in natural fibre composites, Compos Sci Technol 66 (2006) 379–386.
[11] E.O. Momoh, A.I. Osofero, O. Menshykov, Physicomechanical properties of treated oil palm broom fibers for cementitious composites, Journal of Materials in Civil Engineering 32 (10) (2020), 04020300-1-18.
[12] A. Agarwal, B. Nanda, D. Maity, Experimental investigation on chemically treated bamboo reinforced concrete beams and columns, Construction and Building Materials 71 (2014) 610–617.
[13] K. Ghavami, Ultimate Load Behaviour of Bamboo-Reinforced Lightweight Concrete Beams, Cement and Concrete Composites 17 (4) (1995) 281–288.
[14] S. Qaiser, A. Hameed, R. Alyousef, F. Aslam, H. Alabduljabbar, Flexural strength improvement in bamboo reinforced concrete beams subjected to pure bending, Journal of Building Engineering 31 (2020), 101289.
[15] R. Mali, D. Datta, Experimental evaluation of bamboo reinforced concrete slab panels, Construction and Building Materials 188 (2018) 1092–1100.
[16] S.R. Ferreira, M. Pepe, E. Martinelli, F. de Andrade Silva, R. Filho, Inverse identification of the bond behavior for jute fibers in cementitious matrix, Composites Part B: Engineering 95 (2016) 440–452.
[17] A.M. Diab, H.E. Elyamany, M.A. Hussein, H.M. Al Ashy, Bond behavior and assessment of design ultimate bond stress of normal and high strength concrete, Alexandria Engineering Journal 53 (2) (2014) 355–371.
[18] N. Rahman, L.W. Shing, L. Simon, M. Philipp, J. Alireza, H.D. E., C.S. Ling, L. H. Wuan, V. S, S.S. Nee, Enhanced bamboo composite with protective coating for structural concrete application, Energy Procedia 143 (2017) 167–172.
[19] S.Y. Kute, M.R. Wakchaure, Performance Evaluation for Enhancement of Some of the Engineering Properties of Bamboo as Reinforcement in Concrete, Journal of The Institution of Engineers (India): Series A 94 (4) (2013) 235–242.
[20] M. Muhtar, S.M. Dewi, Wisnumurti and A. Munawir, "Enhancing bamboo reinforcement using a hose-clamp to increase bond-stress and slip resistance", *Journal of Building*, Engineering 26 (2019), 100896.
[21] E.O. Momoh, B.I.O. Dahunsi, Suitability of oil-palm-broom-fibres as reinforcement for laterite-based roof tiles, International Journal of Software & Hardware Research in Engineering 5 (4) (2017) 27–35.
[22] E.O. Momoh, A.I. Osofero, Behaviour of oil palm broom fibres (OPBF) reinforced concrete, Construction and Building Materials 221 (2019) 745–761.
[23] E.O. Momoh, A.I. Osofero, A. Martinez-felipe, F. Hamza, Physico-mechanical behaviour of Oil Palm Broom Fibres (OPBF) as eco-friendly building material, Journal of Building Engineering 30 (2020), 101208.
[24] E.O. Momoh, A.I. Osofero, O. Menshykov, Bond behaviour of oil palm broom fibres in concrete for eco-friendly construction, Proceedings of the Institution of Civil Engineers - Construction Materials 174 (1) (2021) 47–64.
[25] E.O. Momoh, A.I. Osofero, O. Menshykov, Bond behaviour of treated natural fibre in concrete, Nano Hybrids and Composites 34 (2022) 37–44.
[26] "ASTM D854-14: Standard Test Methods for Specific Gravity of Soil Solids by Water Pycnometer". ASTM International, West Conshohocken, PA, 2014.
[27] A. D2487, "Standard Practice for Classification of Soils for Engineering Purposes (Unified Soil Classification System)," ASTM International, West Conshohocken, PA, 2017.
[28] ASTM C192/C192M-02: Standard Practice for Making and Curing Concrete Test Specimens in the Laboratory, ASTM International, West Conshohocken, PA, 2016.
[29] "ASTM C496/C496M-17: Standard Test Method for Splitting Tensile Strength of Cylindrical Concrete Specimens". ASTM International, West Conshohocken, PA, 2017.
[30] ASTM C1609/C1609M-12: Standard Test Method for Flexural Performance of Fiber-Reinforced Concrete (Using Beam With Third-Point Loading), ASTM International, West Conshohocken, PA, 2012.
[31] T.J. Looney, M. Arezoumandi, J.S. Volz, J.J. Myers, An experimental study on bond strength of reinforcing steel in self-consolidating concrete, International Journal of Concrete Structures and Materials 6 (3) (2012) 187–197.
[32] A.I. Osofero, M. Corradi, A. Borri, Experimental study of bond strength between titanium bar and lime-based mortar, Journal of Materials in Civil Engineering 27 (6) (2015) 1–10.
[33] K.M.A. Hossain, S. Alam, M.S. Anwar, K.M.Y. Julkarnine, Bond strength of fibre-reinforced polymer bars in engineered cementitious composites, Construction Materials 173 (1) (2020) 15–27.
[34] A. Dey, N. Chetia, "Experimental study of Bamboo Reinforced Concrete beams having", in *International Conference on Processing of Materials*, Minerals and Energy, Ongole, Andhra Pradesh, India, 2016.
[35] M. Kurumatani, Y. Soma, K. Terada, Simulations of cohesive fracture behavior of reinforced concrete by a fracture-mechanics-based damage model, Engineering Fracture Mechanics 206 (2019) 392–407.
[36] Eurocode-2, "EN 1992-1-1: Design of concrete structures - Part 1-1 : General rules and rules for buildings," The European Union Per Regulation 305/2011, Directive 98/34/EC, Directive 2004/18/EC, 2004.
[37] J. Lubliner, J. Oliver, S. Oller, E. Onate, A plastic-damage model for concrete, International Journal of Solids and Structures 25 (3) (1989) 299–326.
[38] J. Lee, G.L. Fenves, Plastic-damage model for cyclic loading of concrete structures, Journal of Engineering Mechanics 124 (8) (1998) 892–900.
[39] B.L. Wahalathantri, D.P. Thambiratnam, T.H.T. Chan, S. Fawzia, "A material model for flexural crack simulation in reinforced concrete elements using ABAQUS", in *Infrastructure, Transport and Urban Development, eddBE2011 Proceedings*, Brisbane, Australia, 2011.
[40] S. Chandrasekaran, P.T.A. Kumar, Damage detection in reinforced concrete berthing jetty using a plasticity model approach, Journal of Marine Science and Application 18 (4) (2019) 482–491.
[41] M. Al-Huri, S. Ahmad, M. Al-Osta, A. Al-Gadhib, M. Kalimur Rahman, Numerical investigation of RC beam strengthened with UHPFRC layers using cohesive surface

bonding method, Assessment and Rehabilitation of Civil Structures, Potsdam, Germany, 2019.
[42] E. Hognestad, Study of combined bending and axial load in reinforced concrete members, University of Illinois at Urbana Champaign, College of Engineering, Illinois, 1951.
[43] B. Zhou, R. Wu, S. Lu, S. Yin, A general numerical model for predicting the flexural behavior of hybrid FRP-steel reinforced concrete beams, Engineering Structures 239 (2021), 112293.
[44] D. J. Carreira and K.-H. Chu, "Stress-strain relationship for plain concrete in compression," *American Concrete Institute (ACI) Journal,* Vols. 82-72, 1985.
[45] A.S. Genikomsou, M.A. Polak, Finite element analysis of punching shear of concrete slabs using damaged plasticity model in ABAQUS, Engineering Structures 98 (1) (2015) 38–48.
[46] D.A. Gujel, C.S. Kazmierczak, J.R. Masuero, Stress-strain curve of concretes with recycled concretea ggregates: analysis of the NBR 8522 methodology, Ibracon Structures and Materials Journal 10 (3) (2017) 547–567.
[47] P. Bamforth, D. Chisholm, J. Gibbs, T. Harrison, Properties of concrete for use in Eurocode 2, The Concrete Centre, Surrey, UK, 2008.
[48] Y. Xiao, Z. Chen, J. Zhou, Y. Leng, R. Xia, Concrete plastic-damage factor for finite element analysis: concept, simulation, and experiment, Advances in Mechanical Engineering 9 (9) (2017) 1–10.
[49] P. Kmiecik, M. Kamiński, "Modelling of reinforced concrete structures and composite structures with concrete strength degradation taken into consideration", *Archives of Civil and mechanical Engineering,* vol, XI 11 (3) (2011) 623–636.
[50] Abaqus documentation, "https://abaqus-docs.mit.edu/2017/English/SIMACAEEXCRefMap/simaexc-c-docproc.htm".
[51] M. Hafezolghorani, F. Hejazi, R. Vaghei, M.S. Bin Jaafar, K. Karimzade, Simplified damage plasticity model for concrete, Structural Engineering International 27 (1) (2017) 68–78.
[52] T. Ozbakkaloglu, A. Gholampour, J.C. Lim, Damage-Plasticity Model for FRP-confined normal-strength and high-strength concrete, Journal of Composites for Construction 20 (6) (2016) 0416053.
[53] M.A. Al-Osta, H.A. Al-Sakkaf, A.M. Sharif, S. Ahmad, M.H. Baluch, Finite element modeling of corroded RC beams using cohesive surface bonding approach, Computers and Concrete 22 (2) (2018) 167–182.
[54] R.D.S.G. Campilho, M.D. Banea, A.M.G. Pinto, L.F.M. da Silva, A.M.P. de Jesus, Strength prediction of single- and double-lap joints by standard andextended finite element modelling, International Journal of Adhesion & Adhesives 31 (5) (2011) 363–372.
[55] A. Ali, A. Lo Conte, C.A. Biffi, A. Tuissi, Cohesive surface model for delamination and dynamic behavior ofhybrid composite with SMA-GFRP interface, International Journal of Lightweight Materials and Manufacture 2 (2) (2019) 146–155.
[56] M. Ramamurthi, J.-S. Lee, S.-H. Yang, Y.-S. Kim, Delamination characterization of bonded interface in polymer coated steel using surface based cohesive model, International Journal of Precision Engineering and Manufacturing 14 (10) (2013) 1755–1765.
[57] A.P. Fantilli, P. Vallini, A cohesive interface model for the pullout of inclined steel fibers in cementitious matrixes, Journal of Advanced Concrete Technology 5 (2) (2007) 247–258.
[58] R. Serpieri, G. Alfano, E. Sacco, A mixed-mode cohesive-zone model accounting for finite dilation and asperity degradation, International Journal of Solids and Structures 67–68 (2015) 102–115.
[59] A. Sakbana, M. Mashreib, Finite element analysis of CFRP- reinforced concrete beams, Revista ingeniería de construcción 35 (2) (2020) 148–169.
[60] N. Chand, M. Fahim, in: Tribology of Natural Fiber Polymer Composites, Elsevier, 2021, pp. 1–59.
[61] E.O. Momoh, A.I. Osofero, O. Menshykov, Enhancing the behaviour of broom-strands reinforced concrete using hose-clamps, Materials Today: Proceedings (2022), https://doi.org/10.1016/j.matpr.2022.03.187. In press.